
Article:
Marensi, E., Ding, Z., Willis, A.P. orcid.org/0000-0002-2693-2952 et al. (1 more author) (2020) Designing a minimal baffle to destabilise turbulence in pipe flows. Journal of Fluid Mechanics, 900. A31. ISSN 0022-1120

https://doi.org/10.1017/jfm.2020.518

Minimal drag forcing to destabilise turbulence in pipe flows

Elena Marensi[1]†, Z. Ding[2], Ashley P. Willis[1], Rich R. Kerswell[2]

[1]School of Mathematics and Statistics, University of Sheffield, Sheffield S3 7RH, UK
[2]Centre for Mathematical Sciences, University of Cambridge, Cambridge CB3 0WA, UK

(Received 4 June 2021)

In our recent theoretical and numerical study of pipe flow transition (Marensi *et al., J. Fluid Mech.*, 2019), we were able to capture the relaminarisation phenomenon observed in the experiments of Kühnen *et al.* (*Flow Turb. Combust., 2018*) due to a flattened base profile. In our simulations, we described the experimental baffle, used to obtain the flattening, as a linear drag force of the form $\mathbf{f}(\mathbf{x},t)=-\chi(\mathbf{x})\mathbf{u}_{tot}(\mathbf{x},t)$, where u_{tot} is total velocity field and $\chi \geqslant 0$ had a prescribed simple spatial distribution. We now optimise the baffle shape by constructing a new fully nonlinear optimisation problem that seeks the 'minimal forcing', i.e. the forcing characterised by the lowest amplitude or the minimum work done against the flow, to just destabilise the turbulence. Starting from N turbulent velocity fields at Reynolds number $Re = 3000$ and suitable initial guesses for the forcing, an optimisation algorithm is developed that is able to optimise the forcing so that the flow completely relaminarises. The corresponding viscous dissipation/wall shear stress is significantly reduced as compared to the unforced (turbulent) case. The resulting optimal forcing, obtained with a variety of different initial guesses and for both short and long pipes, shows a strong radial localisation close to the wall, is axisymmetric and tends to be fairly independent of the streamwise direction, at least for a short pipe. To better understand the optimal streamwise shape/modulation of the forcing, we use an analytical fitting for the optimal radial profile of the forcing and perform a parametric study on the effect of the streamwise extent of the baffle. In the long-pipe case, we find that the energy input is minimised when the baffle is axially localised. Finally, we fix the shape of the baffle to be the optimal found at $Re = 3000$ for long pipes, and study the effect of Reynolds number in the range $Re = 5000$ to 15000. The optimised baffle is able to relaminarise the flow up to $Re = 15000$.

Key words: Variational methods, pipe flow transition

1. Introduction

Skin-friction drag associated with turbulent wall flows is the main contributor to energy losses in a wide variety of industrial and technological applications and thus represents a major cause of increase in operating costs and carbon emissions. In the oil and gas industry, for example, the majority of the pumping cost to transport these fluids in pipes is associated with overcoming the frictional drag at the wall boundary (Keefe 1998). Therefore, any reduction in the turbulent drag, or even the complete suppression of turbulence, would have a tremendous societal impact both from an economic and ecological

† Email address for correspondence: e.marensi@sheffield.ac.uk

viewpoint. Recently a novel method has been designed which achieves such full relaminarisation by just inserting a stationary obstacle in the core of the pipe in order to flatten the incoming turbulent streamwise velocity profile (Kühnen *et al.* 2018b). Surprisingly, this method was shown in the experiments to completely destabilise turbulence, so that the laminar flow was recovered downstream of the baffle and the flow remained laminar thereafter. A first successful step in modelling the experimental baffle was taken by Marensi *et al.* (2019), who theoretically showed the complement of the relaminarisation phenomenon observed in the experiments, i.e. the enhanced nonlinear stability of the laminar state due to a flattened base profile. Our focus here is to optimise this promising control strategy so that as much energy as possible can be saved.

1.1. *Flow control*

Many control strategies have been proposed in the past 50 years, both active (an external energy input is needed) and passive (the flow field is manipulated without any supply of energy). Amongst the active techniques, one of the most popular consists in modifying the near-wall turbulence through large-scale spanwise oscillations created either by a movement of the wall or by a body force (see Quadrio 2011, for a review). For example, Quadrio & Sibilla (2000) were able to achieve 40% drag reduction at a wall Reynolds number $Re_\tau = 172$ by oscillating a pipe around its longitudinal axis, and Auteri *et al.* (2010) reported a drag reduction of 33% at $Re_\tau \approx 200$ by applying a travelling (in the streamwise direction) wave of spanwise velocity at the wall. Passive control strategies includes engineered surfaces, e.g. riblets (e.g. García-Mayoral & Jiménez 2011) and hydrophobic walls (e.g. Min & Kim 2004), and the addition of polymers (e.g. Owolabi *et al.* 2017; Choueiri *et al.* 2018). They have the obvious advantage of requiring no energy input, however, in general, achieve lower drag reduction than active methods.

Ultimately, the goal of turbulence control is to completely extinguish turbulence but, in most cases, none of these techniques are able to achieve so. Temporary relaminarisation phenomena have been reported in pipe and channel turbulent flows under the effect of acceleration, curvature, heating, magnetic field, and stratification (see Sreenivasan 1982, for a review). Interestingly, He *et al.* (2016) obtained relaminarisation in a buoyancy-aided flow (vertical pipe heated from below) and showed that the mean flow was flattened by the buoyancy force. The relaminarisation was attributed to the reduction in the "apparent" Reynolds number of the flow, only related to the pressure force of the flow. A flattened base profile is also characteristic of magnetohydrodynamic duct flows, for which suppression of turbulent fluctuations is a known phenomenon (Krasnov *et al.* 2008).

Relaminarisation is not only alluring because of the huge energy savings it would lead to, but is also a very interesting phenomenon from a fundamental point of view as it requires a profound understanding of the mechanisms of production and dissipation of near-wall turbulence. It is well established that in linearly stable flows, such as pipe flow, transition to turbulence occurs via large transient amplification of perturbations, namely cross-flow disturbances of small amplitude generating large amplitude streamwise velocity perturbations known as streaks (Schmid & Henningson 2001). Transient growth is associated with the so called lift-up mechanism Brandt (2014) in which the vortices lift low-speed fluid from the wall into the fast moving interior, while the high speed fluid is brought down towards the wall. This mechanism is also present in fully turbulent flows, where it accounts for the generation of strong velocity streaks induced by the near-wall quasi-streamwise vortices. For turbulence to be self-sustained, though, feedback mechanisms that generate new vortices must also be present, appended to the streak transient growth. These feedback mechanisms have been discussed, amongst others, by

Waleffe (1997); Jiménez & Pinelli (1999) who suggested that the streamwise vortices are regenerated by a secondary instability of the near wall streaks.

Most of the control methods to suppress turbulence have thus focused on targeting different key structures or stages of the turbulence regeneration cycle in order to interrupt it. For example, Choi *et al.* (1994); Xu *et al.* (2002) developed an opposition control technique aimed at counteracting the streamwise vortices – due to their crucial role in the self-sustained mechanism of turbulence – by wall transpiration in order to achieve drag reduction or even full collapse turbulence. Another class of feedback control strategies targets the streak-instability vortex regeneration mechanism by eliminating or stabilising the near wall low-speed streaks by means of appropriate spanwise forcing of the flow (Du & Karniadakis 2000). These methods, although the most sophisticated and advanced on a theoretical basis, are difficult and expensive to implement as they require small scale sensors and actuators for real time measurements and control of the flow. Furthermore, the transient growth appears to be the primary contributor to the turbulent energy production (Schoppa & Hussain 2002; Tuerke & Jiménez 2013), while the precise manner of the turbulent feedback mechanism is secondary. This suggests that large-scale methods that target the mean shear to counteract/weaken the lift-up mechanism may be the most effective in destroying turbulence. The important role of the mean shear was confirmed by Hof *et al.* (2010) in their relaminarisation experiments of localised turbulence. In transitional pipe flows at relatively low Re, turbulence appears in the form of localised structures, known as puffs, coexisting with the laminar flow. Hof *et al.* (2010) observed that if two puffs were triggered too close to each other, the downstream puff would collapse. They attributed the relaminarisation of the puff to the flattened streamwise velocity profile induced by the trailing puff. The flattening indeed reduces the energy supply from the mean flow to the streamwise vortices, thus subduing the turbulence regeneration cycle beyond recovery. Their findings are also consistent with "Barkley's two-component model" of fully turbulent flow (Barkley *et al.* 2015), where the excitability to the turbulent state was shown to be associated with the streamwise velocity component only, thus suggesting that a suitable (steady) modification of the mean profile may suppress the turbulent state completely.

Inspired by these observations, Björn Hof and his collaborators at the Institute of Science and Technology, Vienna, have conducted a campaign of experiments, whereby the flattening of a turbulent streamwise velocity profile in a pipe flow was shown to lead to a full collapse of turbulence (Kühnen *et al.* 2018; Kühnen *et al.* 2018b, 2019; Scarselli *et al.* 2019) for Reynolds numbers up to 40000, thus reducing the frictional losses by as much as 90%. Different experimental techniques were employed to obtain the flattened base profile – e.g. rotors or fluid injections to increase the turbulence level near the wall, or an impulsive streamwise shift of a pipe segment to locally accelerate the flow – all of them being characterised by a reduced linear transient growth, as compared to the uncontrolled case. It should be noted that the above-quoted highest Reynolds number reported in the experiments was achieved with the wall-movement method, whose applicability, however, is limited by the fact that the shift length, and hence the time needed to flatten the mean profile, increase linearly with Re.

The control technique that we have been focussing on in our study is the experimental baffle described by Kühnen *et al.* (2018b). The baffle decelerates the flow in the middle and accelerates it close to the wall so that the base profile is flattened. As well as not requiring any energy input, this technique is also incredibly simple to implement. With this control scheme, Kühnen *et al.* (2018b) were able to completely relaminarise the flow for Re up to 6000 with the friction drag being reduced by a factor of 3.4 sufficiently downstream of the baffle. For very smooth and straight pipes, the authors observed that,

once relaminarised, the flow would remain laminar 'forever'. For higher Re, e.g. 13000, only a temporary relaminarisation could be achieved, but a 'local' drag reduction of more than 10% could still be obtained in a spatially confined region downstream of the device.

1.2. *Flow optimisation*

In pipes and channels turbulence arises despite the linear stability of the laminar state. The observed transition scenario can thus only be initiated by finite amplitude disturbances (see Eckhardt *et al.* 2007, for a review). The 'smallest' of such disturbances, i.e. the perturbation of lowest energy that can just trigger transition, called the 'minimal seed', provides a measure of the nonlinear stability of the laminar state. It is both of fundamental interest for characterising the basin of attraction of the laminar state, and of practical use, for identifying disturbances that are the 'most dangerous', and therefore need avoiding, when turbulence is undesirable.

In the past twenty years, variational methods have been successfully used to construct fully nonlinear optimisation problems to find the minimal seeds for transition in different flow configurations (e.g., in pipe flow geometry, Pringle & Kerswell 2010; Pringle *et al.* 2012, 2015). In its simplest form the minimal-seed problem can be stated as follows: among all (incompressible) initial conditions of a given perturbation energy E_0, the optimisation algorithm seeks the disturbance that gives rise to the largest energy growth $G(T, E_0)$ for an asymptotically long time T. To find the minimal seed, the initial energy E_0 is gradually increased and the variational problem solved until the critical energy E_c is reached where turbulence is just triggered.

From a control point of view, the ability to quantify the nonlinear stability of the laminar state means that this knowledge can be used to design more nonlinearly stable flows by some manipulation of the system. Indeed, if the critical initial energy for transition of the minimal seed can be shown to increase with some control strategy, then the latter is proved to be effective. This was the idea underlying the study of Rabin *et al.* (2014), where a suitable spanwise oscillation of the wall in Plane Couette flow was shown to increase E_c by 40%.

Based on the same concept, in Marensi *et al.* (2019) we showed enhanced nonlinear stability of a flattened base profile in a pipe, by studying the effect of flattening on the minimal seed. The enhanced nonlinear stability of the laminar state is the complement of the turbulence destabilisation phenomenon observed in Kühnen's experiments. By the no-slip condition, the surfaces of the baffle apply a drag to the flow. Hence, in our simulations, we modelled the obstacle as a simple linear drag force of the form $\mathbf{f}(\mathbf{x}, t) = -\chi(\mathbf{x})\mathbf{u}_{tot}(\mathbf{x}, t)$, where u_{tot} is total velocity field and $\chi \geqslant 0$ is a step function in the streamwise direction and homogeneous in the other directions. Because such forcing does not invoke an active component, it is suitable to model a purely passive control strategy. In Marensi *et al.* (2019) we showed that turbulence can be avoided by this method and both laminar and turbulent frictional drag reductions are achieved. However, the obstacle causes a significant pressure drop locally, as discussed in appendix A.

Here, in an effort to improve the performance of the baffle, we construct a new fully nonlinear optimisation problem, whereby the 'minimal forcing', characterised by the lowest amplitude or the minimum work done against the flow, is sought to just destabilise the turbulence. This optimisation problem can be viewed as the dual of the minimal-seed problem described above. While in Marensi *et al.* (2019) the shape of the forcing was fixed such that the baffle blocks the flow (to some degree) almost uniformly within an axially-localised region of the domain, we now allow the forcing to be any function of space and apply an algorithm to find the optimal spatial dependence.

2. Formulation

We consider the problem of constant mass-flux fluid flow through a straight cylindrical pipe of length L and diameter D. The flow is described using cylindrical coordinates $\{r, \theta, z\}$, where z is aligned with the pipe axis. Length scales are non-dimensionalised by the radius $R = D/2$ of the pipe and velocity components by the centerline velocity $2\,U_b$, where U_b is the constant bulk velocity. We consider a perturbation $\mathbf{u} = \{u_r, u_\theta, u_z\}$ superimposed on the laminar flow $\mathbf{u}_{lam} = U(r)\hat{\mathbf{z}} = (1-r^2)\hat{\mathbf{z}}$ so that the full velocity field is given by $\mathbf{u}_{tot} = \mathbf{u}_{lam} + \mathbf{u}(r, \theta, z, t)$. The flow is subject to a force $\mathbf{f}(\mathbf{x}, t) = -\chi(\mathbf{x})\mathbf{u}_{tot}(\mathbf{x}, t)$ which acts against the flow. Following Marensi *et al.* (2019), the forcing is designed to mimic the drag experienced by the baffle as a linear damping. The problem is governed by the continuity and Navier-Stokes equations

$$\nabla \cdot \mathbf{u} = 0 \tag{2.1}$$

$$\mathbf{NS} = \frac{\partial \mathbf{u}}{\partial t} + U\frac{\partial \mathbf{u}}{\partial z} + u_r U'\hat{\mathbf{z}} - \mathbf{u} \times \nabla \times \mathbf{u} + \nabla p - \frac{4\beta}{Re}\hat{\mathbf{z}} - \frac{1}{Re}\nabla^2\mathbf{u} = \mathbf{f}(\mathbf{x}, t), \tag{2.2}$$

where the prime indicates total derivative, $Re = U_b D/\nu$ is the Reynolds number and $\beta = \beta(\mathbf{u})$ is a correction to the pressure gradient such that the mass flux remains constant. Periodic boundary conditions are imposed in the streamwise direction and no-slip/no-penetration conditions on the pipe walls.

The parameter $1 + \beta$ is an observed quantity in experiments and is defined as:

$$1 + \beta = \frac{\langle \partial p/\partial z \rangle_{turb}}{\langle \partial p/\partial z \rangle_{lam}} \tag{2.3}$$

where the angle brackets indicate the volume integral

$$\langle \bullet \rangle = \int_0^L \int_0^{2\pi} \int_0^1 \bullet \, r \mathrm{d}r \mathrm{d}\theta \mathrm{d}z \,. \tag{2.4}$$

We also introduce a streamwise, an azimuthal and a cylindrical-surface averages as follows

$$\overline{\bullet}^z = \frac{1}{L}\int_0^L \bullet \, \mathrm{d}z \qquad \overline{\bullet}^\theta = \frac{1}{2\pi}\int_0^{2\pi} \bullet \, \mathrm{d}\theta \qquad \overline{\bullet}^{\theta,z} = \frac{1}{2\pi L}\int_0^L \int_0^{2\pi} \bullet \, \mathrm{d}\theta \mathrm{d}z \,, \tag{2.5}$$

as well as a time average

$$\overline{\bullet}^\tau = \frac{1}{\tau}\int_{T-\tau}^{T} \bullet \, \mathrm{d}t \,, \tag{2.6}$$

where T is an asymptotically long time horizon and $0 < \tau \leqslant T$. For $\tau = T$ we indicate the time average over the whole window $[0,\, T]$ as

$$\overline{\bullet} = \frac{1}{T}\int_0^T \bullet \, \mathrm{d}t \tag{2.7}$$

A variational problem is formulated that seeks the optimal forcing $\mathbf{f}(\mathbf{x}, t)$ which just relaminarises the flow. The work done by the forcing *against the flow*, $W(\mathbf{x}, t) = -\mathbf{f} \cdot \mathbf{u}_{tot} = \chi \mathbf{u}_{tot}^2$, has to be positive everywhere in the domain otherwise we would need to compensate for the work done by extracting energy directly from the flow (negative damping). A way to ensure this is to consider $\chi = \phi^2$.

The formulation of the variational problem depends on the choice of the objective functional to optimise in order to relaminarise the flow. The simplest choice is to minimise the total viscous dissipation $\mathcal{D}(\mathbf{u}_{tot}) = Re^{-1}\langle(\nabla \times \mathbf{u}_{tot})^2\rangle$. This method should select

laminar solutions, if they exists. However, the baffle introduces a drag, which needs to be taken into account in the overall energy budget. The key quantity of interest (to be minimised) is thus the total energy input into the flow $\mathcal{I}(\mathbf{u}_{tot};\phi) = \mathcal{D}(\mathbf{u}_{tot}) + \mathcal{W}(\mathbf{u}_{tot};\phi)$, which includes the total work done by the forcing $\mathcal{W} = \langle W \rangle$. In either case, differently from the minimal-seed problem solved by e.g. Pringle *et al.* (2012), the flow is initially turbulent and therefore, in order to smooth the hypersurface of the lagrangian, we need to *time average* the objective functional over a time window $[\tau,\,(T-\tau)]$ taken to be sufficiently long and sufficiently far from the initial time that the flow can be regarded as statistically steady. Furthermore, to avoid sensitivity to initial conditions, we consider $N > 1$ (typically $N = 20$ is found to be sufficient) turbulent fields and perform the optimisation 'averaged' over all of these turbulent fields. The two optimisation problems arising from the different choice of objective functional are formulated in the next two sections. Preliminary tests showed that convergence of the optimisation algorithm was quicker as $\tau \to T$. Hence, the formulations discussed below are presented for the case $\tau = T$, to which all the results presented in §3 will pertain to.

2.1. *Optimisation problem (1): minimise viscous dissipation*

The functional to minimise is:

$$\mathcal{J}_1 = \sum_n \overline{\mathcal{D}}_n(\mathbf{u}_{tot,n}) = \sum_n \frac{1}{T}\int_0^T \frac{1}{Re}\langle(\nabla \times \mathbf{u}_{tot,n})^2\rangle \mathrm{d}t, \tag{2.8}$$

where $\overline{\mathcal{D}}_n(\mathbf{u}_{tot,n})$ is the time-averaged dissipation associated with the n^{th} turbulent field and $\sum_n$ corresponds to $\sum_{n=1}^N$. The above functional is minimised subject to the constraint of the 3D Navier-Stokes equation and constant mass flux and for a given amplitude of the forcing $<\phi^2>=A_0$. Then, motivated by the dual minimal-seed problem, we gradually decrease A_0 until we cannot relaminarise the flow any more and thus we have reached the critical (minimal) amplitude of the forcing A_{cr}. The work done associated with a given χ can be calculated as an observable following the optimisation. The forcing modifies the mean streamwise velocity profile $U_{mean}(r) = (1-r^2) + \overline{u_z}^{\theta,z}$. Another quantity of interest is thus the wall shear stress, relative to the unforced laminar value, namely

$$\frac{\mathcal{S}}{\mathcal{S}_{lam}} = \frac{(\partial_r U_{mean})_{|r=1}}{-2} = 1 - \frac{1}{2}\left.\frac{\partial \overline{u_z}^{\theta,z}}{\partial r}\right|_{r=1} \qquad (\text{with } \partial_r = \partial/\partial r)\,, \tag{2.9}$$

which is a measure of the friction encountered by the flow at the wall. The Lagrangian is:

$$\mathcal{L}_1 = \mathcal{J}_1 + \lambda\left[\langle\phi^2(\mathbf{x})\rangle - A_0\right] + \sum_n \int_0^T \left\langle \mathbf{v}_n \cdot \left[\mathbf{NS}(\mathbf{u}_n) + \phi^2(\mathbf{x})\mathbf{u}_{tot,n}(\mathbf{x},t)\right]\right\rangle \mathrm{d}t \tag{2.10}$$
$$+ \sum_n \int_0^T \langle \Pi_n \nabla\cdot\mathbf{u}_n\rangle \mathrm{d}t + \sum_n \int_0^T \langle \Gamma_n \mathbf{u}_n \cdot \hat{\mathbf{z}}\rangle \mathrm{d}t.$$

In the light of our modelling of the baffle as a linear damping force, the choice of a L_1 norm seems the most reasonable, as it models the distribution of a certain amount of material (an obstacle) in the pipe. Appendix B shows that the results obtained with an L_2-normed distribution are similar. Taking variations of $\mathcal{L}_1$ and setting them equal to zero we obtain the following set of Euler-Lagrange equations for each turbulent field:

Adjoint continuity and Navier-Stokes equations

$$\frac{\delta\mathcal{L}_1}{\delta p_n} = \nabla\cdot\mathbf{v}_n = 0 \tag{2.11a}$$

$$\frac{\delta\mathcal{L}_1}{\delta \mathbf{u}_n} = \frac{\partial \mathbf{v}_n}{\partial t} + U\frac{\partial \mathbf{v}_n}{\partial z} - U' v_{z,n}\hat{\mathbf{r}} + \nabla\times(\mathbf{v}_n\times\mathbf{u}_n) - \mathbf{v}_n\times\nabla\times\mathbf{u}_n + \nabla\Pi_n + \tag{2.11b}$$
$$+\frac{1}{Re}\nabla^2\mathbf{v}_n - \Gamma_n(t)\hat{\mathbf{z}} - \phi^2(\mathbf{x})\mathbf{v}_n + \frac{2}{Re\,T}\nabla^2\mathbf{u}_{tot,n} = 0,$$

Compatibility condition (final condition for backward integration)

$$\frac{\delta\mathcal{L}_1}{\delta\mathbf{u}_n(\mathbf{x},T)} = \mathbf{v}_n(\mathbf{x},T) = 0\,, \tag{2.12}$$

Optimality condition

$$\frac{\delta\mathcal{L}_1}{\delta\phi} = \phi\left(\lambda + \sum_n \sigma_n(\mathbf{x})\right)\,, \tag{2.13}$$

where $\sigma_n(\mathbf{x}) = \int_0^T \mathbf{u}_{tot,n}\cdot\mathbf{v}_n \mathrm{d}t$ is a scalar function of space. The minimisation problem above is solved numerically using an iterative algorithm similar that adopted in Pringle *et al.* (2012) (see their section 2). The update for the next iteration is

$$\phi^{(j+1)} = \phi^{(j)} - \epsilon\frac{\delta\mathcal{L}_1}{\delta\phi^{(j)}} = \phi^{(j)} - \epsilon\phi^{(j)}\left(\lambda + \sum_n \sigma_n^{(j)}(\mathbf{x})\right) = \phi^{(j)} - \gamma\phi^{(j)} - \epsilon\sum_n \sigma_n^{(j)}(\mathbf{x})\phi^{(j)}, \tag{2.14}$$

where $\gamma = \epsilon\lambda$. To find γ (and thus λ) we impose that the updated forcing satisfies the constraint

$$\left\langle [\phi^{(j+1)}]^2(\mathbf{x})\right\rangle = A_0 \implies \left\langle\left[\phi^{(j)}(1-\epsilon\sum_n\sigma_n^{(j)}(\mathbf{x})) - \phi^{(j)}\gamma]^2\right]\right\rangle = A_0. \tag{2.15}$$

The same strategy as Pringle *et al.* (2012) is employed for the adaptive selection of ϵ. Due to the factor ϕ in front of the bracket in (2.14), the choice $\chi = \phi^2$ (or ϕ to any power greater than 1) prevents ϕ from becoming non zero in regions of the domain where it was initially zero (i.e. if ϕ is zero somewhere, it cannot change). This issue is overcome by ensuring that the algorithm is fed with an initial guess for ϕ which is strictly positive everywhere in the domain, as prescribed in §3.1.

2.2. *Optimisation problem (2): minimise the energy input*

The functional to minimise is:

$$\mathcal{J}_2 = \sum_n \overline{\mathcal{I}}_n(\mathbf{u}_{tot};\phi) = \sum_n \underbrace{\frac{1}{T}\int_0^T \frac{1}{Re}\langle(\nabla\times\mathbf{u}_{tot,n})^2\rangle \mathrm{d}t}_{\overline{\mathcal{D}}_n} + \underbrace{\frac{1}{T}\int_0^T \langle\phi^2\mathbf{u}_{tot,n}^2\rangle \mathrm{d}t}_{\overline{\mathcal{W}}_n} \tag{2.16}$$

subject to the constraint of the 3D Navier-Stokes equation and constant mass flux. With this choice of objective functional, we do not need a constraint on the amplitude of the forcing, as the latter appears 'indirectly' in $\mathcal{I}$ (the work done by the forcing can be regarded as proportional to the forcing amplitude). The algorithm, while trying to relaminarise the flow, is allowed to vary (typically decrease) the forcing amplitude in order to minimise both the viscous dissipation and the work done by the forcing at the same time and deliver the optimal forcing straight away. Minimising directly the energy input would thus be more efficient as it avoids the two-step optimisation described for

problem 1 (i.e. minimise $\mathcal{D}$ for fixed A_0 first and then gradually decrease A_0). However, this formulation suffers difficulty with convergence as χ that do not relaminarise the flow can be encountered preventing convergence. We discuss this issue in more detail later. The Lagrangian for this problem is

$$\mathcal{L}_2 = \mathcal{J}_2 + \sum_n \int_0^T \left\langle \mathbf{v}_n \cdot \left[\mathbf{NS}(\mathbf{u}_n) + \phi^2(\mathbf{x})\mathbf{u}_{tot,n}(\mathbf{x},t)\right]\right\rangle \mathrm{d}t + \tag{2.17}$$
$$+ \sum_n \int_0^T \langle \Pi_n \nabla \cdot \mathbf{u}_n \rangle \mathrm{d}t + \sum_n \int_0^T \langle \Gamma_n \mathbf{u}_n \cdot \hat{\mathbf{z}} \rangle \mathrm{d}t$$

and details of the formulation are given in appendix C.

A spectral filtering may also be applied to reduce the noise. The formulations for both optimisation problems with spectral filtering are reported in appendix D for completeness.

2.3. *Numerics*

The calculations are carried out using the open source code openpipeflow.org (Willis 2017), with a variable q discretised in the domain $\{r, \theta, z\} = [0,1]\times[0,2\pi]\times[0,2\pi/\alpha]$ using Fourier decomposition in the azimuthal and streamwise direction and finite difference in the radial direction, i.e.

$$q(r_s, \theta, z) = \sum_{k<|K|} \sum_{m<|M|} q_{s,k,m} e^{i\alpha k z + m\theta} \tag{2.18}$$

where $s = 1, ..., S$ and α is the streamwise wavenumber. The radial points are clustered close to the wall. The optimisation is carried at $Re = 3000$, at which transition is 'clear' and the computational cost of the iterative algorithm still manageable. We consider two cases: one has similar parameters to Pringle *et al.* (2012), i.e. $L = 10R$, $T = 300$ (preliminary tests were carried out to verify that the chosen target time is sufficiently long), and the other one is a long pipe $L = 50R$ $(25D)$ (in order to allow any streamwise localisation) with $T = 100$ (corresponding to $25(D/U_b)$ in advective units) so that the flow passes through the obstacle only once in the chosen optimisation horizon. In this way we expect to help break the axial symmetry of σ (or $\tilde{\sigma}$) due to the translational symmetry of the Navier-Stokes and the adjoint equations, which makes the algorithm move towards a fairly streamwise homogeneous forcing, as we shall discuss later. In the first case we use $S = 60$, $M = 32$, $K = 48$, while for the long-pipe case we use $K = 192$ (and same S and M). In both cases the time step is Δt=0.01.

We also performed DNS for Reynolds number up to 15000 and $L = 50R$, with the spatial and temporal discretisations appropriately increased.

3. The optimal forcing

3.1. *Optimisation problem (1) with $N = 1$ turbulent field*

Our optimisation algorithm was first tested for the case with $N = 1$ turbulent field, which provided suitable initial ϕ for the computationally far more expensive case $N = 20$. A typical turbulent initial condition is shown in figure 1. Following Marensi *et al.* (2019) (refer to their equation 3.5), we start with the initial guess for ϕ,

$$\phi^2 = \chi = A\,\mathcal{B}(z)\,, \tag{3.1}$$

where A is the (scalar constant) amplitude of the forcing and $\mathcal{B}(z)$ is a (scalar) smoothed step-like function that introduces a streamwise localisation of the force. In Marensi *et al.*

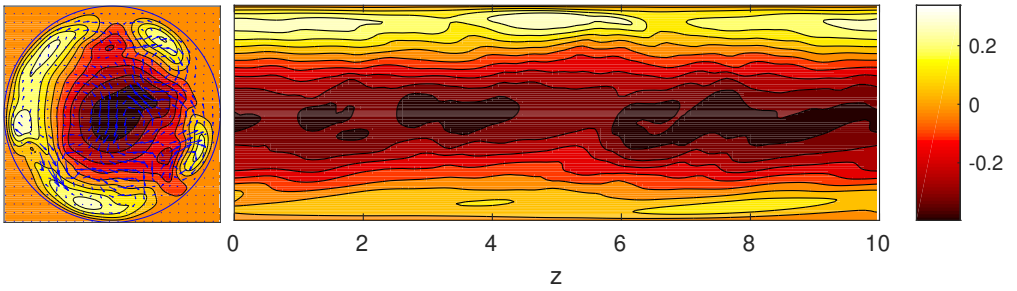

Figure 1: Typical turbulent field used as initial condition in our optimisation algorithm at $Re = 3000$. Cross sections in the $r-\theta$ plane at $z = 0$ (left) and in the $r-z$ plane (figure not in scale) at $\theta = 0$ (right). The contours indicate streamwise velocity perturbations while the arrows in the $r-\theta$ plane correspond to cross-sectional velocities.

(2019) the smoothing function was defined as (Yudhistira & Skote 2011, equation 8):

$$\mathcal{B}(z) = g\left(\frac{z - z_{start}}{\Delta z_{rise}}\right) - g\left(\frac{z - z_{end}}{\Delta z_{fall}} + 1\right), \tag{3.2}$$

with

$$g(z^*) = \begin{cases} 0 & \text{if } z^* \leqslant 0 \\ \{1 + \exp[1/(z^* - 1) + 1/z^*]\}^{-1} & \text{if } 0 < z^* < 1 \\ 1 & \text{if } z^* \geqslant 0 \end{cases}$$

where z_{start} and z_{end} indicate the spatial extent over which the forcing is non-zero, Δz_{rise} and Δz_{fall} are the rise and fall distances of the forcing and $0 \leqslant \mathcal{B}(z) \leqslant 1\ \forall z$. As explained in §2.1, to make sure that the initial guess for χ is strictly positive everywhere we redefine (3.2) as follows: $\mathcal{B}' = (1-b)\mathcal{B} + b$, with $b \geqslant 0$ and $b \leqslant \mathcal{B}'(z) \leqslant 1\ \forall z$. Unless otherwise specified, for the rest of the paper we use $b = 1/3$, so that the initial guess for χ goes to a third at the sides instead of going to zero and the prime will be dropped in the ensuing discussion. The baffle used in Marensi *et al.* (2019) has $z_{start} = 3$, $z_{end} = 7$, $\Delta z_{rise} = \Delta z_{fall} = 1$ and $b = 0$, i.e. it attains its maximal values (i.e. $\mathcal{B} = 1$) over a fifth of a $L = 10R$ long pipe. To check how well our optimisation algorithm performs compared to the available data (the non-optimsed baffle), we perform the optimisation starting from the same spanwise modulation (indicated with $\mathcal{B}_2$ in figure 2(left)) used in Marensi *et al.* (2019). Figure 2(right) shows that the turbulent trajectory is fully relaminarised by the optimised baffle, while it was only 'weakened' by the non-optimised baffle.

Different spanwise modulations have been tested as initial guesses for χ. However, in presenting the results, we will mainly focus on the following two cases (also shown in figure 2(left))

- $\mathcal{B}_1(z)$: $z_{start} = 0$, $z_{end} = 10$, $\Delta z_{rise} = \Delta z_{fall} = 1$ and $b = 1/3$
- $\mathcal{B}_3(z)$: $z_{start} = 4$, $z_{end} = 6$, $\Delta z_{rise} = \Delta z_{fall} = 0.5$ and $b = 1/3$

which corresponds to a very wide and a very thin baffle, respectively. These two 'extreme' cases are considered the most relevant to illustrate the outcomes of our optimisation.
As in Pringle *et al.* (2012), the algorithm was checked for convergence by monitoring the residual and the objective function (time-averaged total dissipation) as the code iterates. A typical example of a converged optimisation in shown in figure 3. The residual has dropped by five orders of magnitude (below 10^{-7}) and the dissipation has flattened out. Note that the jump after approximately 200 iterations is due to the algorithm being

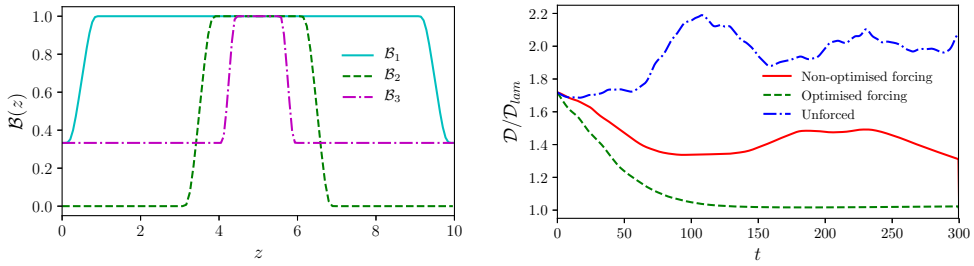

Figure 2: Left: Different spanwise modulations $\mathcal{B}(z)$ of the body force used as initial guesses for χ. The spanwise modulation $\mathcal{B}_2$ corresponds to the non-optimised baffle used in Marensi *et al.* (2019). Right: Effect of the non-optimised (with spanwise modulation corresponding to $\mathcal{B}_2$) and the optimised forcing (fed with the latter as initial guess for ϕ) on a typical turbulent field.

restarted with different parameters (different A_0 and spectral filtering applied in the azimuthal direction) to aid convergence. Furthermore, we also show convergence via reproducibility of the optimal shape, as we shall show in the next section.

Using the L_1-norm to measure the baffle amplitude provides another useful check on convergence. For the optimality condition (2.13) to be satisfied at a given spatial location in the flow either: i) ϕ vanishes (so the baffle is absent there); or ii) $\lambda + \sigma(\boldsymbol{x})$ vanishes (where $\sigma := \sum_n \sigma_n(\boldsymbol{x})$); or iii) both. The fact that relaxing the constraint $\chi = \phi^2 \geqslant 0$ to $\chi = \phi^2 - 1 \geqslant -1$ at any point cannot *increase* the minimum $\mathcal{L}$ (the set of allowable fields is only increasing) means that

$$\frac{\delta \mathcal{L}}{\delta \phi^2} = \lambda + \sigma(\boldsymbol{x}) \geqslant 0 \tag{3.3}$$

at the minimum so then

$$\lambda = \max_{\boldsymbol{x}}(-\sigma(\boldsymbol{x})\,) \tag{3.4}$$

there. As a result $-\sigma(\boldsymbol{x})/\lambda \leqslant 1$ everywhere at convergence with strict equality necessary (but not sufficient) at points where the baffle is present ($\chi > 0$). If $\max_{\boldsymbol{x}}(-\sigma(\boldsymbol{x})\,)$ occurs at isolated points, the baffle takes on the form of a series of δ functions (see appendix E). In contrast, if the set of $\boldsymbol{x}$ which maximize $-\sigma(\boldsymbol{x})$ form a connected domain, the optimal baffle can be degenerate with different optimal baffles having different subsets of support within the domain. (see appendix E). Figure 4 shows the tendency of the algorithm towards this latter situation, with a connected (quasi streamwise-homogeneous) region close to the wall where $-\sigma/\lambda = 1$ (corresponding to where the forcing concentrates, as we shall see later) and only small pockets of the domain where $1 < -\sigma/\lambda \lesssim 2$ indicating convergence is still not complete (initially $-\sigma/\lambda \approx 10$ in places).

These preliminary tests showed that χ tend to be fairly axisymmetric, as expected, given the geometry of the problem. Therefore we apply a spectral filter to filter out $m > 0$ modes. All the results presented hereinafter pertain to the case of an axisymmetric baffle.

3.2. *Optimisation problem (1) with $N = 20$ turbulent fields*

We start from $N = 20$ turbulent fields at $Re = 3000$ and, for the case with $L = 10R$, we consider the two spanwise modulations, $\mathcal{B}_1$ and $\mathcal{B}_3$, with the forcing amplitude appropriately rescaled to the desired A_0. Figures 5 and 6 show the cross sections in the $r - z$ plane of the initial guesses for χ (left) and of the converged structure of χ (right)

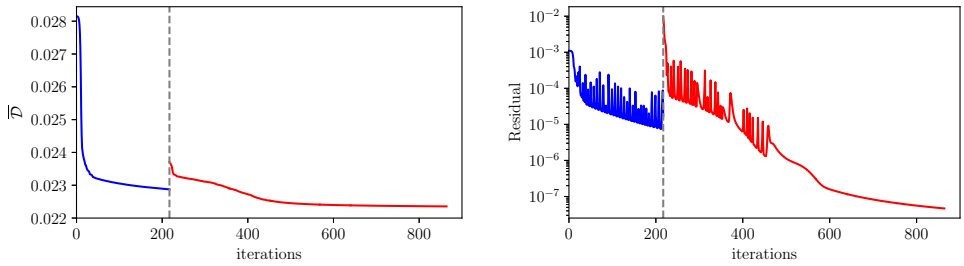

Figure 3: Dissipation (left) and residual (right) vs iterations for the case $\mathcal{B}(3)$ as initial guess and $N = 1$. The jump at iteration 217 is due the algorithm being restarted with different parameters (different A_0 and spectral filtering in the azimuthal direction) to aid convergence.

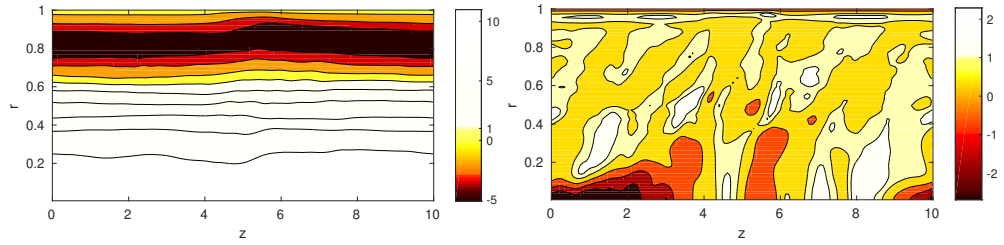

Figure 4: Cross sections of $-\sigma/\lambda$ at the first (left) and last (right) iteration of the case shown in figure 3. The colormap is scaled so that regions where $-\sigma/\lambda > 1$ appear in white.

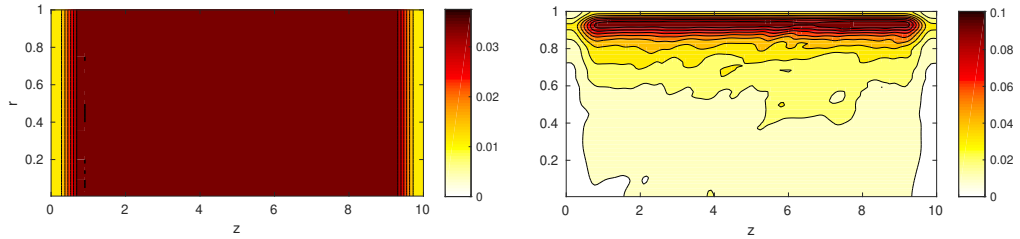

Figure 5: Cross sections in the $r - z$ plane of (left) initial guess for χ and (right) the converged χ (10 levels between zero and the maximum value of χ). Case $L = 10R$, $T = 300$, $\mathcal{B}_1$ as initial guess. The initial amplitude of the forcing is $A_0 = 1.1$.

at the end of the optimisation cycle. In both cases, we observe that χ, which initially is $r-$independent develops a marked radial dependence and is concentrated close to the wall. The streamwise extent of the domain occupied by the forcing, by contrast, has changed little from the initial guesses fed into the algorithm. This may be a reflection of the fact that $\max(-\sigma)$ is only weakly dependent if at all on the streamwise coordinate.

The optimal radial profiles $\overline{\chi}^z(r)$ for the two cases above are displayed in the left graph of figure 7 and they are strikingly similar. In both cases the maximum occurs at a radial location $r \approx 0.8 - 0.9$, where the turbulent production is usually maximum.

These radial profiles are then fed into our algorithm and the optimisation performed with all the modes $k > 0$ filtered out, i.e. χ is restricted to a hypersurface of streamwise-

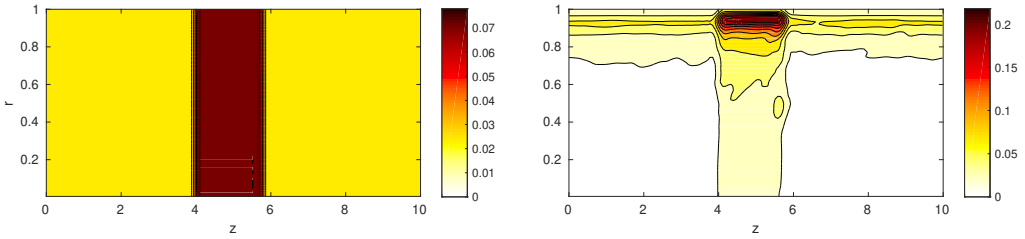

Figure 6: Cross sections in the $r-z$ plane of (left) initial guess for χ and (right) the converged χ (10 levels between zero and the maximum value of χ). Case $L = 10R$, $T = 300$, $\mathcal{B}_3$ as initial guess. The initial amplitude of the forcing is $A_0 = 1.1$.

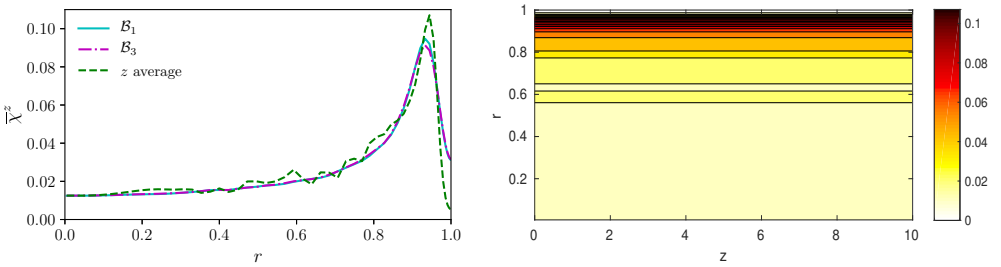

Figure 7: Left: optimal radial profiles of forcings with different streamwise modulations. Right: cross section of the converged χ in the case $L = 10R$, $T = 300$ with all modes filtered out apart from $(0, 0)$. Initial guess given from the radial profiles obtained in the simulations shown in figures 5 and 6.

independent forcings. The $r-z$ cross section of the resulting optimal forcing is shown in figure 7 (right) and its radial profile is added to the left graph of figure 7 for comparison. Its shape is consistent with the other two profiles, with the peak being even more pronounced.

From these calculations, it seems that the algorithm wants to take 'material' from the middle of the pipe and move it close to the wall, then spread it more or less uniformly along the pipe. This is due to the approximate axial symmetry of σ, which is in turn due to the fast advection in a short pipe. We thus tried a longer pipe, $L = 50R$, which, however, was still too short to break the symmetry of σ, at least for optimisation problem (1). Indeed, the results shown in figure 8 are analogous to those obtained with $L = 10R$ and $T = 300$. The optimal radial profile is very similar to its $L = 10R$ counterpart, as shown in figure 8 (right). However, we might be able to break the symmetry by minimising the total input energy, as we shall verify later (section 3.3) by solving optimisation problem (2).

Ultimately we expect the algorithm to find a streamwise localised forcing, if the pipe is sufficiently long. We need to start our optimisation from an initial amplitude of the forcing which is sufficiently large to make the system 'not too noisy' (by ensuring all simulations relaminarise), otherwise the algorithm cannot converge. For this relatively large A_0 our calculations just desrcibed appear to be weakly sensitive to z support, i.e. we can have 'more material' concentrated in a shorter strip of the pipe, or 'less material' spread along the pipe, in both cases localised close to the wall. We might expect the algorithm to pick up the 'optimal,' more localised solution, as we gradually decrease A_0. However, due

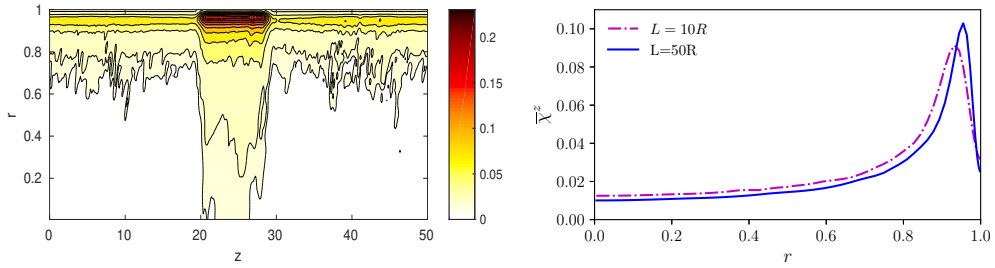

Figure 8: Case $L = 50R$, $T = 100$, $A_0 = 5$. Left: cross section of χ. Right: optimal radial profile compared to the one obtained with $L = 10R$. The optimal solution is converged from a 'stretched' version of $\mathcal{B}_3$ as initial guess for χ

to this insensitivity to the streamwise structure, the algorithm quickly stagnates once it has found the optimal radial profile. Only small adjustments to the radial profile are sufficient to keep the flow laminar as A_0 is gradually decreased. Unexpectedly, this is also the case in the $L = 50R$, as shown in figure 8. If A_0 is decreased too rapidly, a forcing that does not relaminarise the flow might be encountered, thus preventing convergence.

All the results presented above (and others, not shown, with different initial guesses for χ, different spectral filters and formulations) converge to the same optimal radial shape of the baffle and show that our numerics is very quick to organise the structure radially, but not so in the streamwise direction, thus suggesting that the hypersurface of χ is 'quite' flat in the streamwise direction. Therefore, the optimal streamwise modulation/extent is sought 'manually', as it will be shown in the next section.

Moreover, as explained in §2, solving the optimisation problem as a decreasing function of A_0 is time-consuming as A_0 needs to be decreased very gradually otherwise the algorithm does not converge if started from something 'too' turbulent. This procedure was carried out for the streamwise-averaged case in the $L = 10R$-long pipe. Starting from $A_0 = 1.1$ (see figure 7) we were able to decrease the initial amplitude of the forcing down to $A_0 = 0.7$. The optimal radial profile obtained in the latter case is shown in figure 9 and its shape is found to have changed very little from the case with $A_0 = 1.1$ (cfr green dashed lines in figures 7(left) and 9). Therefore, we did not carry out the same procedure for the $L = 50R$ case which is more computationally expensive. The minimum A_0 can instead be directly obtained by solving the optimisation problem that minimises the input energy (see later), with the results from this section being used to have a good initial guess for χ.

3.3. *'Manual' localisation*

To better understand the optimal streamwise structure of the forcing, we use an analytical fitting for the optimal radial profile found in §3.2 and perform a parametric study on the effect of the streamwise extent L_b of the baffle. We consider the optimal radial profile obtained in the $L = 10R$-long pipe for the for the streamwise-averaged case with $A_0 = 0.7$ and we fit the following curve

$$f(r) = [a(e^{br} - 1) + c] \times [\tanh((1 - r)/d)] \tag{3.5}$$

with $a = 0.0000011$, $b = 12$, $c = 0.012$ and $d = 0.071$, as shown in figure 9. The same fitting is used for the case with $L = 50R$ as the optimal profile obtained in this case (also shown in figure 9 left) is very similar to the one obtained for $L = 10R$.

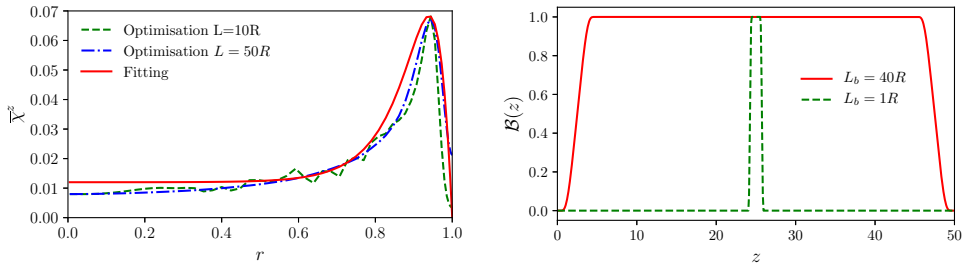

Figure 9: Left: Analytical fitting of the optimal radial profile. The optimised forcings are obtained from a streamwise-averaged optimisation in both $L = 10R$ and $L = 50R$ cases. For the $L = 10R$ case we started from the optimal forcing obtained with $A_0 = 1.1$ (see figure 7) and gradually decreased it to $A_0 = 0.7$. The same procedure was not carried out for $L = 50R$ due to computational expense. Since the radial profile only undergoes small adjustment when the initial amplitude is gradually decreased, a rescaled version from $A_0 \approx 5$ is used in the $L = 50R$ case. Right: Streamwise modulation of the baffle for the cases $L_b = 40R$ and $1R$.

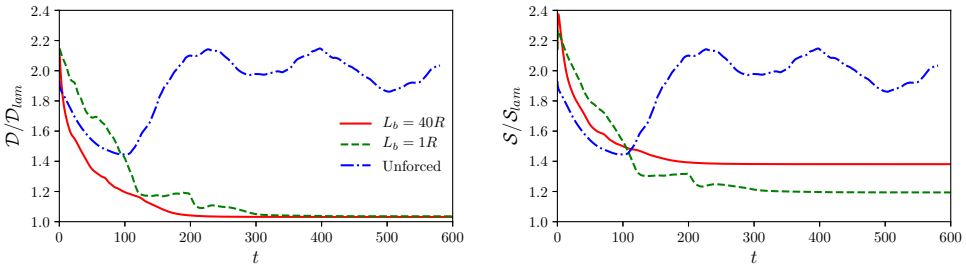

Figure 10: Effect of the baffle length L_b for a $50R$-long pipe. Time series of (left) dissipation and (right) input energy for different streamwise modulations of the forcing at the critical amplitude $A_0 = A_{cr}$ that can just relaminarise the flow.

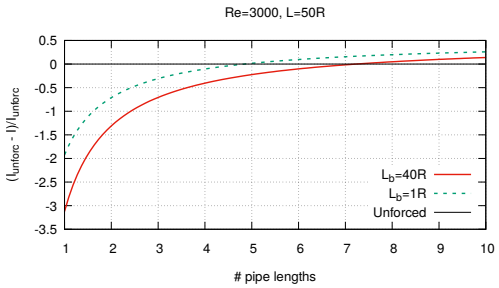

Figure 11: Net energy saving due to optimised baffle at $Re = 3000$ $L = 50R$.

The streamwise modulation of the baffle is introduced using (3.2) and the baffle length L_b is defined as the region where the forcing attains its maximal values, that is $\mathcal{B}(z) = 1$ or, equivalently, $L_b = (z_{end} - z_{start}) - \Delta z_{rise} - \Delta z_{fall}$. The results are only shown for the long-pipe case, where the effect of the baffle localisation is more evident and,

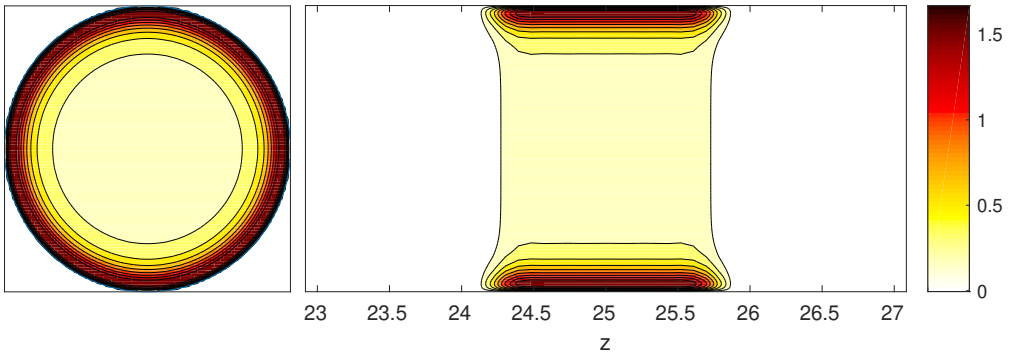

Figure 12: Optimal $\chi(r, z)$ for a $50R$-long pipe. Cross sections in the $r-\theta$ plane at $z = 25$ (where the baffle is localised) and in the $r - z$ plane. Note that the baffle occupies a very small region of the streamwise extent of the pipe and is also radially concentrated close to the pipe walls.

for the rest of the paper, unless otherwise specified, we will assume $L = 50R$. Several streamwise extents and modulations were tested, of which here we present results only for two, most representative, cases: $L_b = 40R$ and $1R$, shown in figure 9 (right). Figure 10 displays the time series of dissipation and input energy for $L_b = 40R$ and $1R$, as well as for the unforced case. The simulations were fed with $N = 5$ different turbulent initial conditions, although the results are presented only for one of them. In both cases the initial amplitude of the forcing was decreased until relaminarisation was not possible anymore, i.e. $A_0 = A_{cr} = 4.3$ (for $L_b = 40R$) and 2.9 (for $L_b = 1R$). Comparison of the long-time asymptotes for the two cases displayed in figure 10 shows that the dissipations decay to an almost identical value, while the wall shear stress reached with the very short baffle after relaminarisation is about half (after subtracting off the laminar unforced value of 1) that obtained with the long baffle. This results in a lower input energy needed with the short baffle compared to the long one. In both cases, the local pressure drop immediately downstream of the baffle is larger than the energy saved by relaminarising the flow. However, assuming the flow remains laminar under nominally perfect pipeline conditions, a downstream distance $L_{even} \geqslant 5$ or 8 pipe lengths ($125D$ or $200D$) is needed in order to achieve a net power saving for the short or long baffle, respectively, as shown in figure 11. This critical length for the short baffle is consistent with the experiments of Kühnen *et al.* (2018b). For a length of the baffle $L_b < 1R$, relaminarisation was not found to be possible. Therefore, the optimal forcing is streamwise localised and in a $50R$-long pipe the minimum extent of the baffle below which the flow cannot be relaminarised is $L_{b,min} = 1R$. The optimal $\chi(r, z)$ is shown in figure 12.

The fact that the dissipations after relaminarisation are almost identical for the very wide and very localised baffles while the input energy is lower for the latter, suggests that we should minimise the input energy (optimisation problem (2)) rather than the dissipation (optimisation problem (1)). At least in the long-pipe case, we should expect the algorithm to converge to a streamwise localised forcing. This is discussed in the following section.

3.4. *Optimisation problem (2)*

In the previous sections we showed that minimising the total viscous dissipation allows us to quickly find the optimal radial shape of the baffle, while clear convergence to an

optimal streamwise structure was not achieved. A parametric study on the effect of the baffle extent showed that a localised baffle can reduce the input energy to a lower value than a wide baffle, the dissipations reached in both cases after relaminarisation being instead very similar. This suggests that minimising the input energy may fix the convergence difficulty of the algorithm in capturing the streamwise localisation of the baffle and motivated us to move onto optimisation problem 2. However, the results obtained solving optimisation problem 2 show that the calculations are still weakly dependent on the z-support, so we do not see streamwise localisation. When the algorithm is fed with a radially homogeneous initial guess like those shown in the left graphs of figures 5 and 6, a forcing which is concentrated close to the wall is obtained, similar to the optimisation problem (1). However, the radial profile is 'less defined' because convergence is more problematic in this case. Indeed, the algorithm tries to decrease the work done by decreasing the amplitude of the forcing. If the amplitude is decreased too much in one step, then some of the turbulent fields might become turbulent again, thus preventing convergence, due to the sensitivity to initial conditions. On the other hand, if fed with a good initial guess for χ (for example obtained from *optimisation problem (1)*), the *optimisation problem (2)* is able to provide the minimum forcing amplitude in a few iterations, much more quickly than by gradually decreasing A_0 with the *optimisation problem (1)*. The optimal radial profile obtained from *optimisation problem (1)* remains almost unchanged when fed into the *optimisation problem (2)* and the critical amplitudes are very close to those obtained 'manually' (see §3.3) for the same extent of the baffle. Therefore, this study, although not able to improve convergence to the optimal streamwise-localised shape, helped us confirming the values of A_{cr} obtained 'manually' in §3.3 for the different baffle extents and it offered a more efficient way of finding such minima than the parametric study of §3.3.

4. Mean profiles

In order to link our results to the experiments of Kühnen *et al.* (2018b), we fix χ to be the optimal form shown in figure 12 and analyse how such baffle modifies the mean streamwise velocity profiles. Figure 13 shows the time series of the energy contained in the azimuthal-independent and azimuthal-dependent modes. Almost all of the relaminarisation happens in the first $t = 25 - 30(D/U_b)$ time units, which means that it occurs in the first pass through the baffle. Indeed, approximately halfway through this time ($t = 12.5 - 15(D/U_b)$), almost exactly half of the pipe is turbulent and the other half laminar, as shown in the iso-contour of figure 14. At $t = 15(D/U_b)$ we analyse the mean profiles along the pipe (see figure 15) and compare with the experimental results of Kühnen *et al.* (2018b) (refer to their figure 7). The incoming flow $z = 10D(20R)$ is very similar to the reference mean turbulent profile. At $z = 12.5D(25R)$ (in the middle of the baffle) we can see little kinks close to the walls , at $z = 22.5D(45R)$ it looks like it is approaching the parabolic profile but it would need a longer pipe to fully reach the parabolic shape. We also present the profile at double the time later $t = 30(D/U_b)$ to show that the profiles just before the baffle are almost parabolic. In comparison to figure 7 of Kühnen *et al.* (2018b), our profiles do not show the overshoots close to the wall, which cause a big pressure drop just downstream of the baffle. Our optimal forcing indeed avoids these M-shaped profiles by being concentrated close to the wall. It is also interesting to analyse the shape of the forcing to compare it with the artificial forcing used in Kühnen *et al.* (2018b) and Marensi *et al.* (2019) (see fig. 2b), which was positive near the wall and negative in the centre. Our forcing, instead, is negative everywhere, i.e. it is decelerating the flow, so it is realisable with a purely passive control method (an

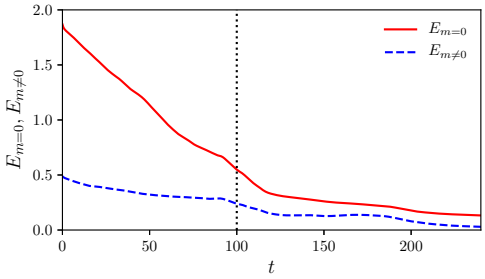

Figure 13: $Re = 3000$, $L = 25D(50R)$, optimal baffle. Time series of energy in $m = 0$ and $m \neq 0$ (azimuthal-dependent) modes. Almost all of the relaminarisation happens in the first $t = 25 - 30(D/U_b)$ time units.

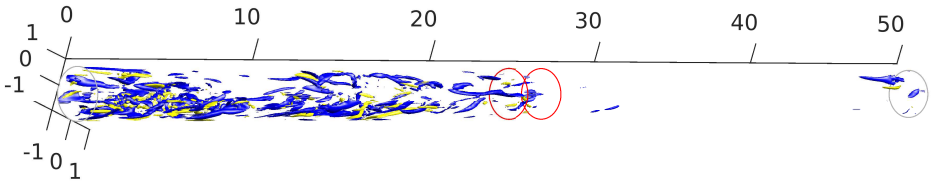

Figure 14: $Re = 3000$, $L = 25D(50R)$, baffle occupies the region between $12D(24R)$ and $13D(26R)$. Isocontours of streamwise vorticity (20% of the max/min)at $t = 15(D/U_b)$.

obstacle). Also it has a plateu in the middle and overshoots close to the walls, possibly in order to kill the near-wall turbulence regeneration cycle.

5. Dependence on Re

The solution of optimisation problem (1), combined with a parametric study on the baffle extent L_b, provided the optimal forcing at $Re = 3000$. The latter is axisymmetric, concentrated close to the wall and streamwise localised too, at least in long pipes ($L = 50R$). Since it would be too expensive to repeat the optimisation procedure at higher Re, we now keep the radial shape of the forcing fixed (as the one shown in figure 9) and rescale either A_0 or L_b to investigate how far – in Re – we can push the relaminarisation phenomenon. All the results presented herein pertain to the case $L = 50R$ and we consider four Reynolds numbers $Re = 5000$, 7000, 10000 and 150000. In the following, we define a skin-friction drag reduction in the laminar and turbulent case as:

$$\mathcal{FR}_{lam/turb} = \frac{\mathcal{S}_{turb} - \mathcal{S}^A_{lam/turb}}{\mathcal{S}_{turb}} \,. \tag{5.1}$$

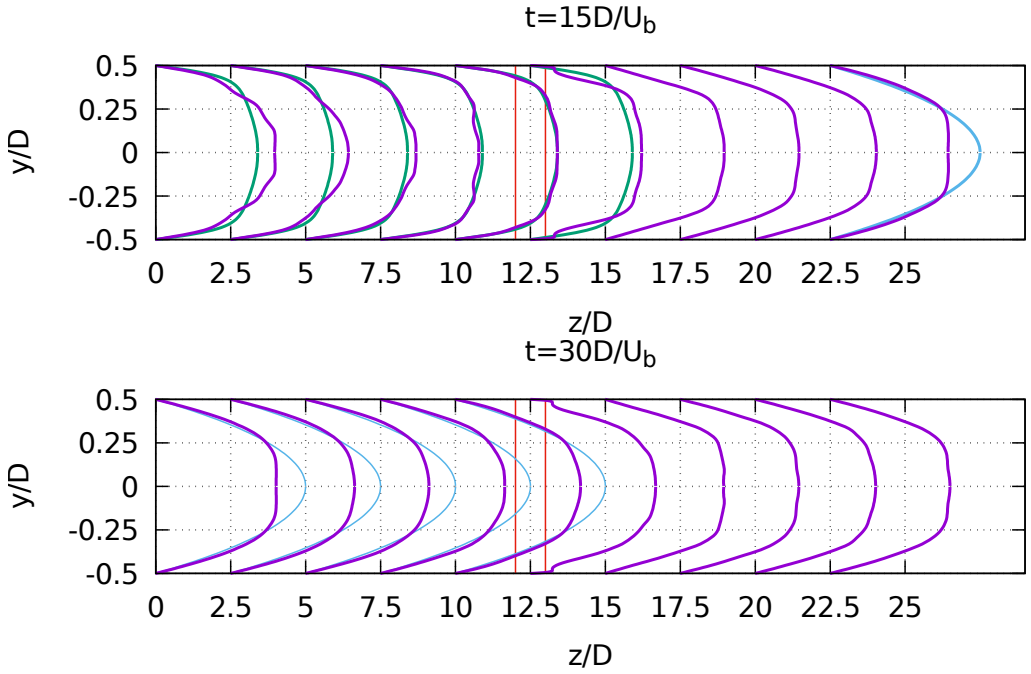

Figure 15: $Re = 3000$, $L = 25D(50R)$, baffle occupies the region between $12D(24R)$ and $13D(26R)$, indicated with red vertical lines. Mean velocity profiles along the pipe at $t = 15(D/U_b)$ (top) and $t = 30(D/U_b)$ (bottom). For $t = 15(D/U_b)$, at $z = 12.5D$ (in the middle of the baffle) we can see little kinks close to the walls, at $z = 22.5D$ it looks like it is approaching the parabolic profile but it would need a longer pipe to fully reach the parabolic shape. The green profiles are the reference (turbulent unforced streamwise averaged) profile, the light blue profiles are the parabolic profile.

where the superscript "A" indicates the forced case and no superscript indicates the unforced case. Note, however, that $\mathcal{FR}_{lam/turb}$ does not take into account the pressure drop downstream of the baffle. The energy saving is given by total drag reduction

$$\mathcal{DR}_{lam/turb} = \frac{\mathcal{I}_{turb} - \mathcal{I}^A_{lam/turb}}{\mathcal{I}_{turb}} = \frac{(1+\beta)_{turb} - (1+\beta)^A_{lam/turb}}{(1+\beta)_{turb}}\,. \tag{5.2}$$

Using Blasius's approximation (Blasius 1913), $\mathcal{I}_{turb}/\mathcal{I}_{lam} = \mathcal{S}_{turb}/\mathcal{S}_{lam} = 0.00494375Re^{0.75}$. Typically, $\mathcal{DR} < 0$ immediately downstream of the baffle. However, in the relaminarised cases, assuming the flow stays laminar, we can evaluate the critical downstream distance L_{even} needed in order to achieve a net power saving ($\mathcal{DR} > 0$).

We first focused on the case $Re = 5000$. Starting from an amplitude of the forcing greater than the critical A_0 at $Re = 3000$, we gradually increased A_0 until relaminarisation was obtained. Figure 17 (left) shows that a forcing amplitude $6 < A_{cr} < 8$ is needed in order to relaminarise the flow, which is more than double the critical amplitude at $Re = 3000$. However, a considerable reduction of the wall shear stress is achieved. As observed for $Re = 3000$ (results not shown), even when the amplitude of the forcing is not large enough to relaminarise the flow, i.e. $A_0 < A_{cr}$, we are still able to reduce the wall shear stress and the flow exhibits an interesting periodic time behaviour, which may suggest shadowing of a periodic orbit. Analogous results were found for $Re = 7000$ and 10000.

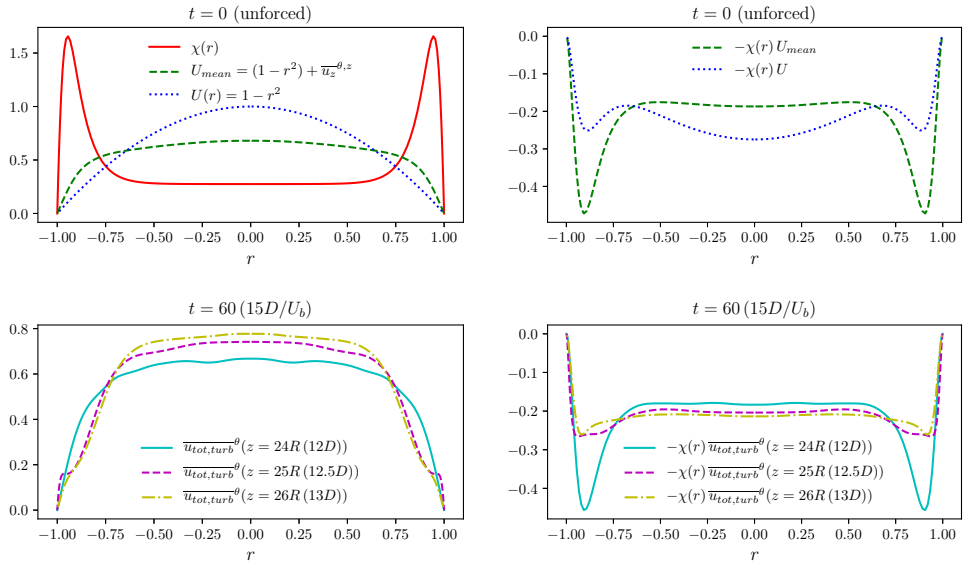

Figure 16: $Re = 3000$, $L = 50R\,(25D)$, baffle occupies the region between $24R\,(12D)$ and $26R\,(13D)$. Form of the forcing in the cases of turbulent and laminar flow. For all cases $\chi(r) = \chi_{opt}(r, z = 25R\,(12.5D))$.

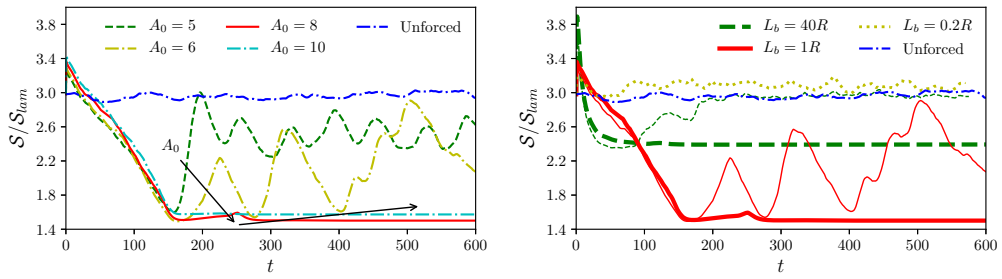

Figure 17: Time series of wall shear stress at $Re = 5000$ in the case $L = 50R$. Left: effect of A_0 for fixed $L_b = 1R$ and the 'optimal' radial shape found in §3.2 for $Re = 3000$. Right: effect of L_b, thick line is for $A_0 > A_{cr}$, thin line is for $A_0 < A_{cr}$.

At $Re = 5000$ we also verified that the streamwise localised baffle ($L_b = 1R$) is still the 'optimal', i.e. it is able to reduce the wall shear stress more than the longer baffle ($L_b = 40R$), as shown in figure 17 (right). Furthermore the long baffle cannot produce any skin-friction turbulent drag reduction when $A_0 < A_{cr}$. As for $Re = 3000$, there is a minimum extent of the baffle $0.2R < L_{b,min} < 1R$ below which relaminarisation is not possible. For $L_b < L_{b,min}$ the wall shear stress in the forced case is higher than in the unforced case.

Therefore, we fix $L_b = 1R$ and apply this optimal forcing to 5 different turbulent initial conditions at $Re = 5000$, 7000 and 10000. For $Re = 15000$, only one turbulent initial condition was used to limit the computational cost. Figure 18 shows that after appropriate rescaling of A_0 a full collapse of turbulence is obtained up to $Re = 15000$.

Figure 19 shows the wall shear stress and skin-friction drag reduction as we gradually

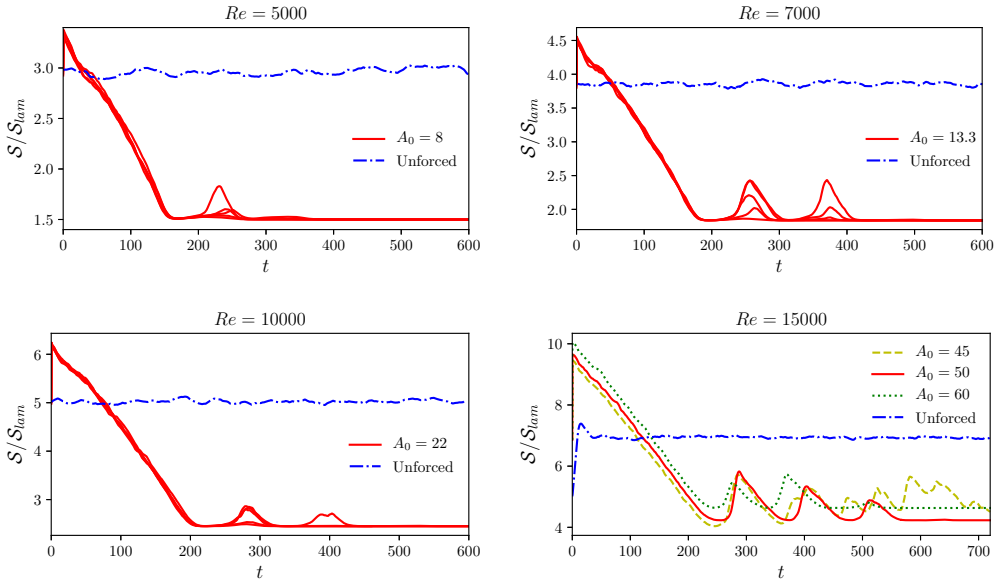

Figure 18: Time series of wall shear stress for different Reynolds number in the case $L = 50R$. The forcing is fixed as the one shown in figure 12.

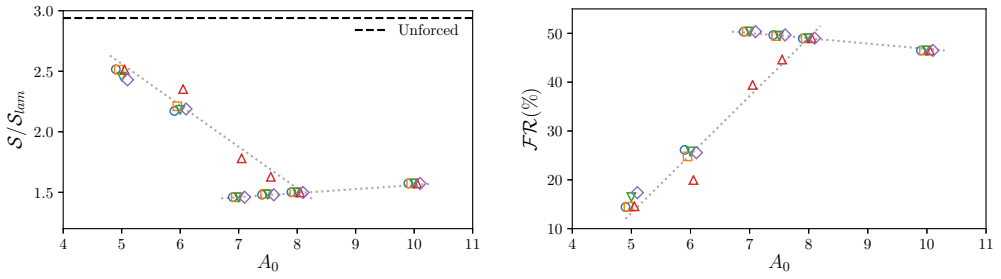

Figure 19: Wall shear stress and skin-friction drag reduction vs A_0 for the case $Re = 5000$ and for 5 turbulent initial conditions. The black dashed line in the left graph indicates the Blasius approximation for a turbulent unforced flow, while the dotted gray lines are drawn to guide the eye.

increase A_0 for the case $Re = 5000$. The critical amplitude is defined in our study as the amplitude for which all turbulent initial conditions relaminarise and it divides the curve of $\mathcal{FR}$ (or $\mathcal{S}/\mathcal{S}_{lam}$) vs A_0 in two branches: for $A_0 < A_{crit}$ skin-friction turbulent drag reduction is obtained, for $A_0 > A_{crit}$ we have skin-friction laminar drag reduction. In this case $A_{crit} = 8$. Note, however, that at this critical amplitude for relaminarisation, $L_{even} \geqslant$ 10 pipe lengths ($250D$). Figure 20 shows that A_0 needs to be increased by an order of magnitude from $Re = 3000$ to $Re = 15000$ in order to obtain relaminarisation. Both the skin-friction laminar and turbulent drag reductions also increase with Re up to $Re =$ 10000. However, the increase in A_0 with Re is also accompanied by an (approximately linear) increase in the critical length L_{even} for a net energy saving, as shown in figure 21. For a downstream distance $z \geqslant L_{even}$, drag reduction is obtained.

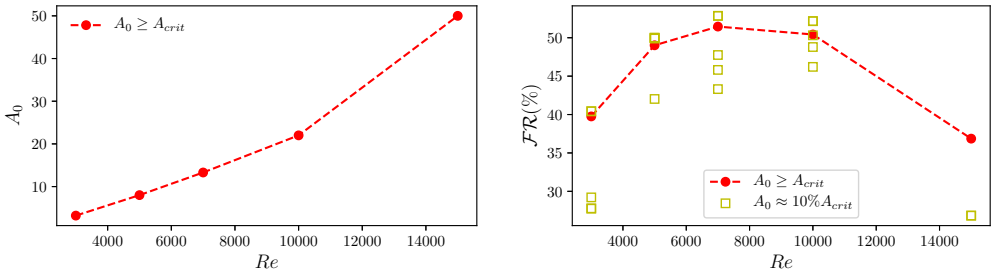

Figure 20: Left: Forcing amplitude A_0 just above (can relaminarise *all* given turbulent initial fields) the critical value amplitude A_{cr} as a function of the Reynolds number Re. Right: the corresponding skin-frictionlaminar drag reduction. The skin-friction turbulent drag reductions obtained for $A_0 = 10\%A_{crit}$ also shown with symbols for the five initial conditions considered at each Re.

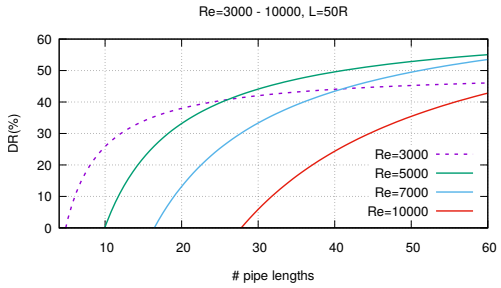

Figure 21: Total drag reduction as a function of the downstream distance from the baffle, in units of pipe length L, for different Re at $A_0 = A_{crit}$. The intersections of the curves with the $x-$axis correspond to the critical downstream distances L_{even} at different Re.

6. Conclusions

Motivated by recent experimental (Kühnen *et al.* 2018b) and numerical (Marensi *et al.* 2019) studies of forced relaminarisation in a pipe flow, in this paper, by combining variational methods with numerical simulations, we have tackled the problem of finding the optimal forcing to just destabilise the turbulence. The complete suppression of turbulence was obtained in the experiments of Kühnen *et al.* (2018b) by inserting a stationary obstacle in the core of the pipe that flattens the incoming turbulent streamwise velocity profile. The drag force exerted by the experimental baffle was modelled in our simulations as $\mathbf{f}(\mathbf{x},t)=-\chi(\mathbf{x})\mathbf{u}_{tot}(\mathbf{x},t)$, where $\mathbf{u}_{tot}$ is the total (laminar flow plus perturbation) velocity field and $\chi(\mathbf{x}) \geqslant 0$ measures, as a function of space, how "intensely" the flow is blocked. An optimisation algorithm was developed and numerically solved at $Re = 3000$ in order to find the optimal spatial distribution of $\chi(\mathbf{x})$. The variational problem was formulated as a minimisation problem for the total viscous dissipation $\mathcal{D}(\mathbf{u}_{tot})$, averaged over a sufficiently long time window T, subject to the constraints of the three-dimensional continuity and Navier-Stokes equations and constant mass flux, for a given amplitude of the forcing $A_0 = \langle\chi(\mathbf{x})\rangle$, where the angle brackets indicate volume average. The forcing amplitude was then gradually decreased until the critical amplitude A_{cr} for relaminarisation was reached, below which turbulence could not be suppressed. We considered two pipe lengths: $L = 10R$ and $L = 50R$, where R is the radius of the pipe. In both cases,

starting from $N > 1$ (typically $N = 20$) turbulent velocity fields and suitable initial guesses for $\chi(\mathbf{x})$, the algorithm converged to an optimal shape of the forcing characterised by a strong radial concentration close to the wall and symmetry around the pipe axis, but was found to be slow in organising the streamwise structure. Therefore, the optimal streamwise extent of the baffle L_b was sought manually by fitting and analytical radial profile to the optimal one found by the optimisation algorithm and performing DNS with different L_b. The input energy, which in the forced case has to balance not only the viscous dissipation but also the work done by the forcing against the flow, was monitored in order to quantify the benefit of the baffle. In the long-pipe case, a streamwise localised baffle was found to save more energy than a wide baffle, with a minimum L_b of approximately $1R$, below which relaminarisation was not possible. Even with a short baffle, however, a net power saving could not be achieved immediately after the obstacle, due to the large pressure drop. A laminar section of flow of approximately $125D$ downstream of the baffle was needed in order to obtain an energy gain. Next, we studied the effect of the Reynolds number in the case $L = 50R$. We fixed the shape of the baffle to be the optimal one found at $Re = 3000$ and performed DNS in the range $Re = 5000 - 15000$, starting from five different turbulent initial conditions. After suitable rescaling of the forcing amplitude, the optimised baffle, was found to fully relaminarise the flow up to $Re = 15000$ (corresponding to $Re_\tau \approx 450$). However, the downstream distance from the baffle needed to achieve a net power saving also increases with Re. This is consistent with the experiments of Kühnen *et al.* (2018b) and with the fact that we are introducing a strong pressure drop locally.

Our results showed that this purely passive method can relaminarise the flow up to relatively high Reynolds number but is not very energy efficient. Other, more general, types of forcing $\mathbf{f} = \boldsymbol{\phi}(\mathbf{x}, t)$, with an active component (i.e. $\boldsymbol{\phi}$ can be positive) might lead to a better performance and increased energy savings. Optimising such forcing is the subject of our current research.

7. Acknowledgements

This work was funded by EPSRC grant EP/P000959/1. Fruitful discussions with Björn Hof and Davide Scarselli are kindly acknowledged.

Appendix A. Corrigendum of Marensi *et al.*, *J. Fluid Mech.*, 2019

In Marensi *et al.* (2019) we investigated whether the flow can be kept laminar in the presence of a baffle modelled as a drag force $\mathbf{F}(r, \theta, z, t) = -A\,\mathcal{B}(z)\,\mathbf{u}_{tot}(r, \theta, z, t)$, where A is the (scalar constant) amplitude of the forcing, $\mathcal{B}(z)$ is a (scalar) smoothed step-like function (refer to (3.2)) that introduces a streamwise localisation of the force and $\mathbf{u}_{tot}(r, \theta, z, t)$ is the total velocity field. The presence of the baffle causes a pressure drop downstream, which is measured by $(1+\beta)^A_{lam/turb} = \mathcal{I}^A_{lam/turb}/\mathcal{I}_{lam}$, where $\mathcal{I}^A_{lam/turb}$ is the input energy needed to drive the flow in either the laminar or turbulent case and $\mathcal{I}_{lam}$ is the corresponding laminar value in the unforced case. The superscript 'A' indicates the forced case ($A > 0$) and the subscripts 'lam' or '$turb$' refer to the flow being laminar (initial perturbation energy E_0 below the critical initial energy for transition E_c, i.e. $E_0 < E_c$) or turbulent ($E_0 > E_c$) at the current value of $A \geqslant 0$.

From the energy balance, it follows that in the forced case the input energy has to compensate both the viscous dissipation $\mathcal{D}$ and the work done by the forcing $\mathcal{W}$. By definition, in the unforced case $\mathcal{W} = 0$ and $(1+\beta)_{turb} \equiv \mathcal{I}_{turb}/\mathcal{I}_{lam} = \mathcal{D}_{turb}/\mathcal{D}_{lam}$. Furthermore, $(1+\beta)^A_{lam/turb} = (\mathcal{D}+\mathcal{W})^A_{lam/turb}/\mathcal{D}_{lam}$. A laminar/turbulent drag reduction

Re	$(1+\beta)_{turb}$	$\mathcal{S}_{lam}^{A=0.005}/\mathcal{S}_{lam}$	$\mathcal{FR}_{lam}$	$(1+\beta)_{lam}^{A=0.005}$	$\mathcal{DR}_{lam}$
2400	1.695	1.143	32.5%	1.59	6%
3500	2.250	1.202	46.5%	1.87	17%
5000	2.940	1.275	56.6%	2.2	25%
7000	3.783	1.354	64.2%	2.68	29%
10000	4.944	1.48	70%	3.35	32%

Table 1: Effect of a forcing of amplitude $A = 0.005$ at different Reynolds numbers (corrigendum of table 3 in Marensi *et al.* (2019)).

$$\mathcal{DR}_{lam/turb} = \frac{\mathcal{I}_{turb} - \mathcal{I}^A_{lam/turb}}{\mathcal{I}_{turb}} = \frac{\mathcal{D}_{turb} - (\mathcal{D}+\mathcal{W})^A_{lam/turb}}{\mathcal{D}_{turb}} = \frac{(1+\beta)_{turb} - (1+\beta)^A_{lam/turb}}{(1+\beta)_{turb}}\,, \tag{A 1}$$

is thus introduced as a measure of the net energy saving (corrigendum of equation (3.7) of Marensi *et al.* (2019)), where $(1+\beta)_{turb}$ is evaluated using Blasius formula (Blasius 1913) as reported in §5. Another quantity of interest is the wall shear stress $\mathcal{S}/\mathcal{S}_{lam}$, relative to the unforced laminar value, defined in (2.9), and the corresponding skin friction drag reduction $\mathcal{FR}_{lam/turb}$ defined in (5.1). The latter does not take into account the pressure drop due to the baffle, however, it is a measure of how much friction the flow encounters at the wall. Note that, in the unforced case, $(1+\beta)_{turb} \equiv \mathcal{I}_{turb}/\mathcal{I}_{lam} = \mathcal{D}_{turb}/\mathcal{D}_{lam} = \mathcal{S}_{turb}/\mathcal{S}_{lam}$.

In the Reynolds number range $Re = 2400$ to 10000, for a $5D$-long pipe, starting from initial conditions just above the laminar-turbulent boundary in the unforced case we first investigated whether a forcing of very small amplitude ($A = 0.005$) could avoid turbulence being triggered, i.e. expand the basin of attraction of the base flow. The values reported in the third and fourth columns of table 3 of Marensi *et al.* (2019) do not refer to $(1+\beta)_{lam}^{A=0.005}$ and $\mathcal{DR}_{lam}$, as reported in Marensi *et al.* (2019), but instead to $\mathcal{S}^A_{lam}/\mathcal{S}_{lam}$ and $\mathcal{FR}_{lam}$. The corrected labels as well as the actual values of $(1+\beta)_{lam}^{A=0.005}$ and $\mathcal{DR}_{lam}$ are shown in the amended table 1.

At $Re = 5000$ we performed a parametric study on the amplitude A of the forcing. The labels on the vertical axes in the bottom graph of figure 11 of Marensi *et al.* (2019) should read $\mathcal{S}/\mathcal{S}_{lam}$ on the left and $\mathcal{FR}(\%)$ on the right (see corrected figure 22), with the caption and the ensuing discussion being revised accordingly. Unfortunately, at $A = 0.01$ the actual energy input $(1+\beta)_{turb}^{A=0.01} = 3.36$ is already higher than in the unforced case and β increases approximately linearly with A. At $A = 0.03$, where a full collapse of turbulence is achieved, $(1+\beta)_{turb}^{A=0.03} = 7.73$. However, assuming the flow remains laminar under nominally perfect pipeline conditions, sufficiently downstream of the baffle (or periodic array of baffles), a net energy saving will be achieved.

Appendix B. Optimisation using L_2 norm

The formulation using L_2 norm is presented in the following. The Lagrangian becomes:

$$\mathcal{L}_1 = \overline{\mathcal{D}}(\mathbf{u}) + \lambda\left[\langle\chi^2(\mathbf{x})\rangle - A_0\right] + \int_0^T \langle \mathbf{v}\cdot[\mathbf{NS}(\mathbf{u}) + \chi(\mathbf{x})\mathbf{u}_{tot}(\mathbf{x},t)]\rangle\,\mathrm{d}t + ... \tag{B 1}$$

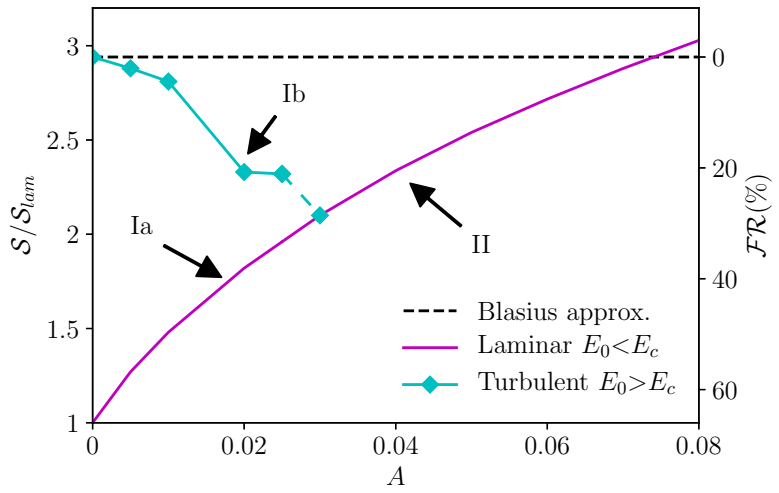

Figure 22: Effect of the forcing for different A at $Re = 5000$: wall shear stress and skin-friction drag reductions vs forcing amplitude. For $A < 0.03$ either laminar (Ia: $E_0 < E_c$) or turbulent (Ib: $E_0 > E_c$) skin-friction drag reductions are possible, for $A \geqslant 0.03$ turbulence is suppressed (corrigendum of bottom graph of figure 11 in Marensi *et al.* (2019)).

The gradient and the update for the next iteration are:

$$\frac{\delta \mathcal{L}_1}{\delta \chi} = 2\lambda\chi(\mathbf{x}) + \sigma(\mathbf{x}) = 0 \tag{B 2}$$

$$\chi^{(j+1)} = \chi^{(j)} - \epsilon \frac{\delta \mathcal{L}_1}{\delta \chi^{(j)}} = \chi^{(j)} - \epsilon \left[2\lambda\chi^{(j)}(\mathbf{x}) + \sigma^{(j)}(\mathbf{x})\right], \tag{B 3}$$

All the rest is unchanged. To ensure the update is non-negative, (B 3) is replaced by:

$$\chi^{(j+1)} = \max\left\{0, \chi^{(j)} - \epsilon[2\lambda\chi^{(j)} + \sigma^{(j)}]\right\} \tag{B 4}$$

To find λ we impose that $\left\langle [\chi^{(j+1)}(\mathbf{x})]^2 \right\rangle = A_0$ and we employ a bracketing method (e.g. the regula falsi algorithm) to find the root λ of $g(\lambda) = \left\langle \left[\chi^{(j+1)}(\mathbf{x})\right]^2 \right\rangle - A_0 = \left\langle [\max\left\{0, \chi^{(j)} - \epsilon(2\lambda\chi^{(j)} + \sigma^{(j)})\right\}]^2 \right\rangle - A_0 = 0$.

Figure 23 shows a comparison of the optimal forcing obtained using L_1 and L_2 norms starting from the initial guess shown in figure 6(left). The optimal radial profiles (left) are similar, both presenting the radial concentration close to the wall. The one obtained using the L_2 norm is slightly less peaked, as it is reasonable to expect. The formulation with L_2 norm is also found to be weakly dependent on the $z-$support, as shown in the $r - z$ cross section on the right.

Appendix C. Formulation for optimisation problem (2)

By taking variations of the lagrangian given in (2.17) and setting them equal to zero we obtain the following set of Euler-Lagrange equations:

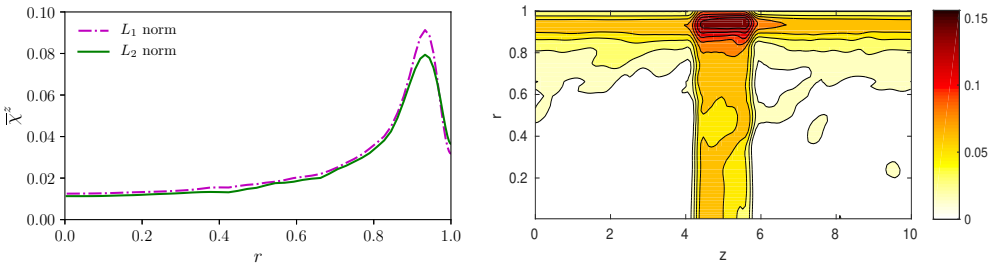

Figure 23: Case $L = 10R$, $T = 300$, with $\mathcal{B}_3$ as initial guess. Comparison of the optimal forcing obtained using L_1 and L_2 norms. Left: optimal radial profile $\chi(r)$. The L_2-normed distribution (purple dash-dotted curve) is the same shown in figure 7 with the same colour/line style. Right: $r - z$ cross section.

Adjoint continuity and Navier-Stokes equations

$$\frac{\delta \mathcal{L}_2}{\delta p_n} = \nabla \cdot \mathbf{v}_n = 0 \tag{C 1a}$$

$$\frac{\delta \mathcal{L}_2}{\delta \mathbf{u}_n} = \frac{\partial \mathbf{v}_n}{\partial t} + U\frac{\partial \mathbf{v}_n}{\partial z} - U' v_{z,n}\hat{\mathbf{r}} + \nabla \times (\mathbf{v}_n \times \mathbf{u}_n) - \mathbf{v}_n \times \nabla \times \mathbf{u}_n + \nabla \Pi_n + \tag{C 1b}$$
$$+ \frac{1}{Re}\nabla^2 \mathbf{v}_n - \Gamma_m(t)\hat{\mathbf{z}} - \phi^2(\mathbf{x})\mathbf{v}_n + \frac{2}{Re\,T}\nabla^2 \mathbf{u}_{tot,n} - \frac{2}{T}\phi^2 \mathbf{u}_{tot,n} = 0,$$

Compatibility condition

$$\frac{\delta \mathcal{L}_2}{\delta \mathbf{u}_n(\mathbf{x}, T)} = \mathbf{v}_n(\mathbf{x}, T) = 0, \tag{C 2}$$

Optimality condition

$$\frac{\delta \mathcal{L}_2}{\delta \phi} = \phi \sum_n \tilde{\sigma}_n(\mathbf{x}) = 0, \tag{C 3}$$

where

$$\tilde{\sigma}_n(\mathbf{x}) = \int_0^T \mathbf{u}_{tot,n} \cdot \left(\frac{\mathbf{u}_{tot,n}}{T} + \mathbf{v}_n \right) \mathrm{d}t \tag{C 4}$$

is a scalar function of space. The update for the next iteration is

$$\phi^{(j+1)} = \phi^{(j)} - \epsilon \frac{\delta \mathcal{L}_2}{\delta \phi^{(j)}} = \phi^{(j)} - \epsilon \phi^{(j)} \sum_n \tilde{\sigma}_n^{(j)}(\mathbf{x}) = \phi^{(j)}[1 - \epsilon \sum_n \tilde{\sigma}_n^{(j)}(\mathbf{x})]. \tag{C 5}$$

Note that with this optimisation problem we still have the issue that if $\phi = 0$ initially, it cannot change.

Appendix D. Spectral filtering

D.1. *Optimisation problem (1)*

A spectral filtering on ϕ is implemented by adding a constraint to the lagrangian, namely

$$\mathcal{L}_1 = \sum_n \overline{\mathcal{D}}_n(\mathbf{u}_n) + \lambda \left[\langle \phi^2(\mathbf{x})\rangle - A_0\right] + \xi \left\langle \phi - \mathcal{F}(\phi)\right\rangle + ..., \tag{D 1}$$

where $\mathcal{F}$ is the spectral filtering operator. Using the linearity of $\mathcal{F}$, it is straightforward to show that the above filtering constraint is equivalent to applying the filter to the gradient $\delta\mathcal{L}_1/\delta\phi$, that is

$$\mathcal{F}\left(\frac{\delta \mathcal{L}_1}{\delta \phi}\right) = \mathcal{F}\left[\phi\left(\lambda + \sum_n \sigma_n(\mathbf{x})\right)\right] = 0, \tag{D 2}$$

where $\sigma_n(\mathbf{x}) = \overline{\mathbf{u}_{tot,n}\cdot\mathbf{v}_n}$ is a scalar function of space. The update is thus:

$$\phi^{(j+1)} = \phi^{(j)} - \epsilon\mathcal{F}\left[\phi^{(j)}\left(\lambda + \sum_n \sigma_n^{(j)}(\mathbf{x})\right)\right] = \phi^{(j)} - \gamma\phi^{(j)} - \epsilon\mathcal{F}\left(\sum_n \sigma_n^{(j)}\phi^{(j)}\right), \tag{D 3}$$

where $\gamma = \epsilon\lambda$ and $\mathcal{F}(\phi^{(j)}) = \phi^{(j)}$. In order to find γ (and thus λ) we impose that $\langle[\phi^{(j+1)}]^2\rangle = \langle[\phi^{(j)} - \epsilon\mathcal{F}(\sum_n \sigma_n^{(j)}\phi^{(j)}) - \phi^{(j)}\gamma]^2\rangle = A_0$.

D.2. *Optimisation problem (2)*

With the filter $\phi = \mathcal{F}(\phi)$ the optimality condition becomes:

$$\mathcal{F}\left(\frac{\delta \mathcal{L}_2}{\delta \phi}\right) = \mathcal{F}\left[\phi\sum_n \tilde{\sigma_n}\right] = 0. \tag{D 4}$$

so that the update is:

$$\phi^{(j+1)} = \phi^{(j)} - \epsilon\mathcal{F}\left(\frac{\delta\mathcal{L}}{\delta\phi^{(j)}}\right) = \phi^{(j)} - \epsilon\mathcal{F}\left(\phi^{(j)}\sum_n \tilde{\sigma}_n^{(j)}\right) = \mathcal{F}(\phi^{(j+1)}). \tag{D 5}$$

Appendix E. The L_1 amplitude condition

To understand the significance of the set of $\boldsymbol{x}$ which maximize $-\sigma(\boldsymbol{x})$, we generalise the L_1 amplitude constraint used in the main body of the paper to

$$\|\chi\|_\alpha := \left(\frac{1}{V}\int \chi^\alpha dV\right)^{1/\alpha} = \frac{A_0}{V} = a \tag{E 1}$$

so that limit $\alpha \to 1$ recovers the L_1 condition. The modified Lagrangian becomes

$$\begin{aligned}\mathcal{L}_1 = \ldots + \lambda\left[V\left(\frac{1}{V}\int\chi^\alpha dV\right)^{1/\alpha} - A_0\right] + \sum_n \int_0^T \langle \mathbf{v}_n\cdot[\ldots + \chi(\mathbf{x})\mathbf{u}_{tot,n}(\mathbf{x},t)]\rangle\,\mathrm{d}t + \ldots \\ - \int \mu(\boldsymbol{x})(\chi - \gamma^2)dV\end{aligned} \tag{E 2}$$

where the requirement that χ is positive semidefinite is now explicitly imposed. Setting variations with respect to χ, μ and γ to zero gives respectively

$$\lambda\,\alpha\,a^{1-\alpha}\chi^{\alpha-1} + \sigma - \mu = 0, \tag{E 3}$$

$$\chi - \gamma^2 = 0, \tag{E 4}$$

$$2\mu\gamma = 0. \tag{E 5}$$

Equation (E 5) makes it clear that either: i) $\gamma = 0$ (so $\chi = 0$ and $\sigma = \mu$); or ii) $\mu = 0$; or iii) both if σ happens to vanish. The baffle therefore can only exist when $\gamma(\boldsymbol{x}) \neq 0$ which requires $\mu(\boldsymbol{x}) = 0$ (although the opposite is not true) and in this case, the relations (E 1), (E 3)-(E 5) simplify to just (E 1) and (E 3) rearranged as follows

$$\left(\frac{1}{V}\int \left[\frac{\chi}{a}\right]^{\alpha} dV\right)^{1/\alpha} = 1 \tag{E 6}$$

$$\left[\frac{\chi}{a}\right]^{\alpha-1} = \frac{-\sigma}{\alpha\lambda} \tag{E 7}$$

substituting (E 7) into (E 6) gives

$$\alpha\lambda = \|-\sigma\|_{1/\varepsilon} := \left[\frac{1}{V}\int (-\sigma)^{1/\varepsilon} dV\right]^{\varepsilon} \tag{E 8}$$

where $\varepsilon := (\alpha - 1)/\alpha$ goes to 0^+ as $\alpha \to 1^+$ and then

$$\frac{-\sigma}{\alpha\lambda} = \frac{-\sigma}{\|-\sigma\|_{1/\varepsilon}}. \tag{E 9}$$

At this point, it is worth stressing that $\sigma = \sigma(\boldsymbol{x};\varepsilon)$ and assuming the simple regular expansion

$$\sigma(\boldsymbol{x};\varepsilon) = \sigma_0(\boldsymbol{x}) + \varepsilon\sigma_1(\boldsymbol{x}) + O(\varepsilon^2) \tag{E 10}$$

where $\sigma_0(\boldsymbol{x})$ is the distribution calculated in §3.1, then

$$(-\sigma)^{1/\varepsilon} = (-\sigma_0(\boldsymbol{x}))^{1/\varepsilon} e^{\sigma_1(\boldsymbol{x})/\sigma_0(\boldsymbol{x}) + O(\varepsilon)}. \tag{E 11}$$

In the limit as $\varepsilon \to 0$, it follows that $\lambda \to \max(-\sigma_0(\boldsymbol{x}))$ and so $-\sigma_0(\boldsymbol{x})/\lambda \leqslant 1$ as discussed in §3.1. For the baffle structure, there are two scenarios - either σ_0 achieves its global maximum at isolated points or there are finite domains over which this is achieved. Consider the former first. (E 7) is

$$\left[\frac{\chi}{a}\right]^{\alpha} = \frac{(-\sigma)^{1/\varepsilon}}{\frac{1}{V}\int (-\sigma)^{1/\varepsilon} dV} \tag{E 12}$$

If $-\sigma_0^* = \max(-\sigma_0)$ occurs at an isolated point $\boldsymbol{x}^*$, then

$$\frac{1}{V}\int (-\sigma)^{1/\varepsilon} dV \approx c\varepsilon^{d/2} e^{\sigma_1(\boldsymbol{x}^*)/\sigma_0^*} (-\sigma_0^*)^{1/\varepsilon} \tag{E 13}$$

using Laplace's method in d dimensions and letting c gather all the known constants together. So

$$\left[\frac{\chi}{a}\right]^{\alpha} = \frac{1}{c\varepsilon^{d/2}} e^{\sigma_1(\boldsymbol{x})/\sigma_0(\boldsymbol{x}) - \sigma_1(\boldsymbol{x}^*)/\sigma_0^*} \left[\frac{-\sigma_0(\boldsymbol{x})}{-\sigma_0^*}\right]^{1/\varepsilon} \tag{E 14}$$

which, as $\varepsilon \to 0$ ($\alpha \to 1$), either tends to zero if $\boldsymbol{x} \neq \boldsymbol{x}^*$ or diverges to infinity at $\boldsymbol{x} = \boldsymbol{x}^*$ in such a way that the volume integral is finite. Hence the baffle structure is a δ-function or a collection of δ-functions around the set of isolated $\boldsymbol{x}^*$ which globally maximize $-\sigma_0(\boldsymbol{x})$.

The alternate, and more plausible, scenario is that $-\sigma_0$ is maximized over a connected set $\Lambda := \{\boldsymbol{x} \,|\, -\sigma_0(\boldsymbol{x}) = \max(-\sigma_0)\}$ (or sets). Then (E 14) is replaced by

$$\left[\frac{\chi}{a}\right]^{\alpha} \approx \frac{e^{\sigma_1(\boldsymbol{x})/\sigma_0(\boldsymbol{x})}}{\int_\Lambda e^{\sigma_1(\boldsymbol{x})/\sigma_0^*} dV} \left[\frac{-\sigma_0(\boldsymbol{x})}{-\sigma_0^*}\right]^{1/\varepsilon} \tag{E 15}$$

as $\varepsilon \to 0$. Assuming $\mu = 0$ over Λ, the baffle then has a smooth structure over Λ generated by $\sigma_1(\boldsymbol{x})$ (*a posteriori* justification for adopting the simple regular expansion in (E 10)). However, there can be subsets of Λ over which $\mu \neq 0$ where the baffle vanishes. This possibility allows for a non-uniqueness of the optimal baffle which can only exist on the intersection of the set where $\mu = 0$ and Λ.

REFERENCES

Auteri, F., Baron, A., Belan, M., Campanardi, G. & Quadrio, M. 2010 Experimental assessment of drag reduction by traveling waves in a turbulent pipe flow. *Phys. Fluids* **22** (11), 115103.

Barkley, D., Song, B., Mukund, V., Lemoult, G., Avila, M. & Hof, B. 2015 The rise of fully turbulent flow. *Nature* **526**, 550–553.

Blasius, H. 1913 Das ähnlichkeitsgesetz bei reibungsvorgängen in flüssigkeiten. In *Mitteilungen über Forschungsarbeiten auf dem Gebiete des Ingenieurwesens*, pp. 1–41. Springer.

Brandt, L. 2014 The lift-up effect: the linear mechanism behind transition and turbulence in shear flows. *Eur. J. Mech.-B/Fluids* **47**, 80–96.

Choi, H., Moin, P. & Kim, J. 1994 Active turbulence control for drag reduction in wall-bounded flows. *J. Fluid Mech.* **262**, 75–110.

Choueiri, G. H., Lopez, J. M. & Hof, B. 2018 Exceeding the asymptotic limit of polymer drag reduction. *Phys. Rev. Lett.* **120** (12), 124501.

Du, Y. & Karniadakis, G. E. 2000 Suppressing wall turbulence by means of a transverse traveling wave. *Science* **288** (5469), 1230–1234.

Eckhardt, B., Schneider, T. M., Hof, B. & Westerweel, J. 2007 Turbulence transition in pipe flow. *Ann. Rev. Fluid Mech.* **29**, 447–468.

García-Mayoral, Ricardo & Jiménez, Javier 2011 Drag reduction by riblets. *Phil. Trans. Royal Soc. A* **369** (1940), 1412–1427.

He, S., He, K. & Seddighi, M. 2016 Laminarisation of flow at low Reynolds number due to streamwise body force. *J. Fluid Mech.* **809**, 31–71.

Hof, B., De Lozar, A., Avila, M., Tu, X. & Schneider, T. M. 2010 Eliminating turbulence in spatially intermittent flows. *Science* **327** (5972), 1491–1494.

Jiménez, J. & Pinelli, A. 1999 The autonomous cycle of near-wall turbulence. *J. Fluid Mech.* **389**, 335–359.

Keefe, L. R. 1998 Method and apparatus for reducing the drag of flows over surfaces. US Patent 5,803,409.

Krasnov, D., Zikanov, O., Schumacher, J. & Boeck, T. 2008 Magnetohydrodynamic turbulence in a channel with spanwise magnetic field. *Phys. Fluids* **20** (9), 095105.

Kühnen, J., Scarselli, D.e & Hof, B. 2019 Relaminarization of pipe flow by means of 3d-printed shaped honeycombs. *J. Fluids Eng.* **141** (11), 111105.

Kühnen, J., Scarselli, D., Schaner, M. & Hof, B. 2018b Relaminarization by steady modification of the streamwise velocity profile in a pipe. *Flow Turbul. Combust.* pp. 1–25.

Kühnen, J., Song, B., Scarselli, D., Budanur, N. B., Riedl, M., Willis, A. P., Avila, M. & Hof, B. 2018 Destabilizing turbulence in pipe flow. *Nat. Phys.* **14**, 386–390.

Marensi, E., Willis, A. P. & Kerswell, R. R. 2019 Stabilisation and drag reduction of pipe flows by flattening the base profile. *J. Fluid Mech.* **863**, 850–875.

Min, T. & Kim, J 2004 Effects of hydrophobic surface on skin-friction drag. *Phys. Fluids* **16** (7), L55–L58.

Owolabi, B. E., Dennis, D. J. C. & Poole, R. J. 2017 Turbulent drag reduction by polymer additives in parallel-shear flows. *J. Fluid Mech.* **827**.

Pringle, C. C. T. & Kerswell, R. R. 2010 Using nonlinear transient growth to construct the minimal seed for shear flow turbulence. *Phys. Rev. Lett.* **105**, 154502.

Pringle, C. C. T., Willis, A. P. & Kerswell, R. R. 2012 Minimal seeds for shear flow turbulence: using nonlinear transient growth to touch the edge of chaos. *J. Fluid Mech.* **702**, 415–443.

Pringle, C. C. T., Willis, A. P. & Kerswell, R. R. 2015 Fully localised nonlinear energy growth optimals in pipe flow. *Phys. Fluids* **27**, 064102.

Quadrio, M. 2011 Drag reduction in turbulent boundary layers by in-plane wall motion. *Phil. Trans. R. Soc. Lond. A* **369** (1940), 1428–1442.

Quadrio, M. & Sibilla, S. 2000 Numerical simulation of turbulent flow in a pipe oscillating around its axis. *J. Fluid Mech.* **424**, 217–241.

Rabin, S. M. E., Caulfield, C. P. & Kerswell, R. R. 2014 Designing a more nonlinearly stable laminar flow via boundary manipulation. *J. Fluid Mech.* **738**, 1–12.

Scarselli, D., Kühnen, J. & Hof, B. 2019 Relaminarising pipe flow by wall movement. *J. Fluid Mech.* **867**, 934–948.

Schmid, P. J. & Henningson, D. S. 2001 *Stability and Transition on Shear Flows*, , vol. 142. Springer Science & Business Media.

Schoppa, W. & Hussain, F. 2002 Coherent structure generation in near-wall turbulence. *J. Fluid Mech.* **453**, 57–108.

Sreenivasan, K. R. 1982 Laminarescent, relaminarizing and retransitional flows. *Acta Mech* **44** (1-2), 1–48.

Tuerke, F. & Jiménez, J. 2013 Simulations of turbulent channels with prescribed velocity profiles. *J. Fluid Mech.* **723**, 587–603.

Waleffe, F. 1997 On a Self-Sustaining Process in shear flows. *Phys. Fluids* **9**, 883–900.

Willis, A. P. 2017 The Openpipeflow Navier–Stokes solver. *SoftwareX* **6**, 124–127.

Xu, C.-X., Choi, J.-I. & Sung, H. J. 2002 Suboptimal control for drag reduction in turbulent pipe flow. *Fluid dynamics research* **30** (4), 217–231.

Yudhistira, I. & Skote, M. 2011 Direct numerical simulation of a turbulent boundary layer over an oscillating wall. *J. Turb.* (12), N9.